Joint Centre for Mesoscale Meteorology, Reading, UK

A Study of the Effects of Horizontal and Vertical Resolution in the New Dynamics representation of FASTEX IOP16

Humphrey Lean

Internal Report No. 132
NWP Scientific Paper No. 64

October 2001

Met Office Joint Centre for Mesoscale Meteorology Department of Meteorology
University of Reading PO Box 243 Reading RG6 6BB United Kingdom
Tel: +44 (0)118 931 8425 Fax: +44 (0)118 931 8791
www.metoffice.com

Designed and produced by the Met Office © Crown copyright 2001 01/0240 The Met Office logo is a registered trademark.

A Study of the Effects of Horizontal and Vertical Resolution in the New Dynamics representation of FASTEX IOP16

October 2001

Humphrey Lean

Abstract

An important question which needs to be addressed when developing high resolution (1-10km) models is what resolution (both horizontal and vertical) is required in order to correctly represent various atmospheric phenomena. In this report a systematic study of some of the effects of using different horizontal gridlengths and different vertical resolutions in the New Dynamics model is presented. Simulations have been carried out of the FASTEX IOP16 rapidly developing cyclone case with 60,24,12,4 and 2km gridlengths. Extra features which appear on reducing the gridlength are discussed and the effect on larger scale features is also considered. An analysis of the effect of different gridlengths in terms of energy spectra is also presented as are comparisons of the models with observations. In addition work is presented on increasing the vertical resolution in 4 and 2km models. It is found that in the 2km model increasing the vertical resolution leads to realistic splitting of the cross frontal slantwise circulations.

1. Introduction

An important question which needs to be addressed when developing high resolution (1-10km) models is what resolution (both horizontal and vertical) is required in order to correctly represent various atmospheric phenomena. In this report a systematic comparison of some of the effects of using different horizontal gridlengths between 60 and 2km in New Dynamics simulations of FASTEX IOP16 are presented. In addition work is presented on increasing the vertical resolution in 4 and 2km models. The two main themes are what is gained in each increase in resolution in terms of new structures resolved and the effect on the large scale fields – i.e. comparison of the fields averaged up to lower resolutions. Section 2 briefly introduces the case and model runs and Section 3 looks at the effects of horizontal resolution on the dynamic fields. Section 4 presents similar results on the microphysics and precipitation fields. Section 5 discusses the comparison of the various horizontal resolutions with observations. Section 6 presents comparisons of the models with different vertical resolutions and Section 7 compares the different vertical resolution with observations.

2. The case and models

Both the case and the model configurations used in this study have been extensively reported elsewhere so only the essential and relevant information is given here and the reader is referred to references for further details. The FASTEX Intensive Observations Period (IOP) 16 was a rapidly developing, rapidly moving secondary cyclone case. More details of the case are given in Forbes et al (2000). The system develops rapidly from 0Z on 17th Feb 1997 (at which point there is virtually no surface system) until 12Z on the same day. The main times of interest are 6-12Z since those are the times during which the UK C-130 dropped sondes into the system during a systematic survey flight. The main point of scientific interest in the system is the multiple slantwise cross frontal circulations driving multiple cloud heads.

2.1 Model Configurations used for the Horizontal Resolution Study

The configurations of the New Dynamics model used in this case (and the reasoning behind them) are discussed by Lean (2000). The model runs discussed in the first sections of this report dealing with horizontal resolution were carried out with 45 vertical levels which correspond to a separation of approx. 300m in the mid troposphere. . It might be expected that this is not sufficient for the 4 and 2km runs (and this is confirmed when the work varying the vertical resolution was carried out) but it was considered important to not produce a consistent set of runs with varying horizontal resolution but with a fixed vertical level separation.

The 60km run discussed here was a global run which was initialised from a UM operational global analysis at 0Z. In order to ensure consistency (although it may not

have been strictly necessary) the 12km UM analysis was transplanted into the global one over the domains of the higher resolution models. The 24 and 12km runs were both run over the same area using the 12km UM analysis as the starting data and boundary conditions generated from the 60km global run. The 4 and 2km runs also used the same 12km starting data but used boundary conditions derived from the 12km and 4km runs respectively. The 4km and 2km runs were repeated with the effect of the convection scheme suppressed by setting the CAPE closure timescale to a very long value (10^6s). These runs are discussed in more detail in Lean (2000).

An important feature of the high resolution (4 and 2km) runs is that not only were they run from 12km analyses at 0Z but there was also no assimilation of observations and also no orography (or other land based information) since the case took place over the Atlantic Ocean. This means that no high resolution information is being put into the model runs so all the structure generated with 4 and 2km gridlengths is being generated by the model. This case is therefore an important test of the internally generated structures before we move on to work on cases involving orography or assimilation in which additional high resolution information *is* being put in.

2.2 Model Configurations used in vertical resolution study

In order to carry out a systematic investigation of the effect of increasing the vertical resolution it was decided to approximately double the resolution of the 45 level model to 90 levels. The set of levels chosen is shown in figure 2.1 compared to the 45 levels. The levels were generated using a quadratic dependence for eta with stretching at the top to avoid too many levels being put near the top of the model. This gives a resolution in the mid troposphere of about 150m. In addition a few 2km runs have been carried out with the vertical resolution enhanced by another factor of 1.5 giving 135 levels with approx. 100m spacing in the mid troposphere.

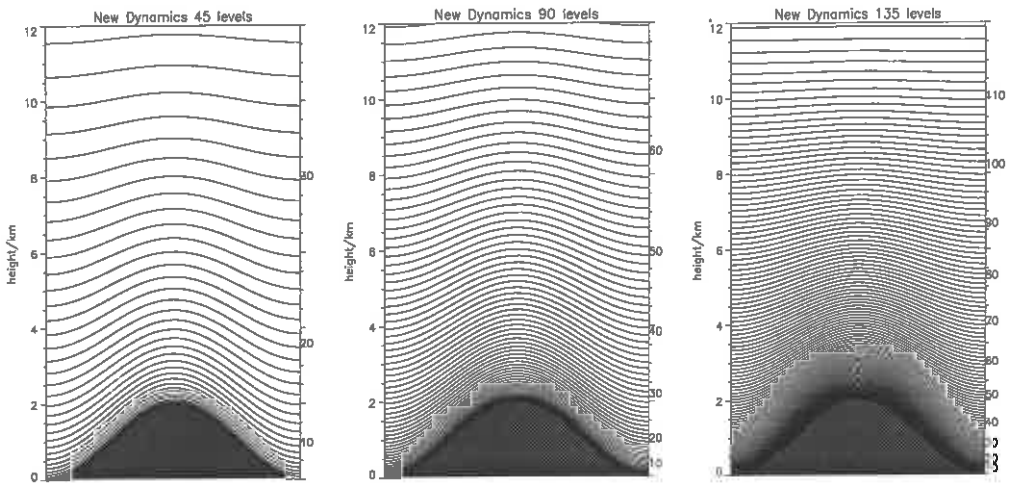

Figure 2.1 Comparison of 45, 90 and 135 level sets (theta levels shown).

The models run with increased vertical resolution had a horizontal resolution of 4 or 2km. The 4km model was nested within the 12km, 45 level model described in the previous section. In order to nest the 4km model within the 12km one the boundary conditions needed to be interpolated in the vertical from 45 levels to the new 90. Once the 4km, 90 level model was running the 2km 90 level one was simply nested within that. The 2km 135 level run used the same boundary data as the 2km, 90 level run interpolated in the vertical from 90 to 135 levels. The 4km model was usually run with the convection scheme switched on and a CAPE closure timescale of 1200s. The 2km model was usually run with the convection scheme switched off.

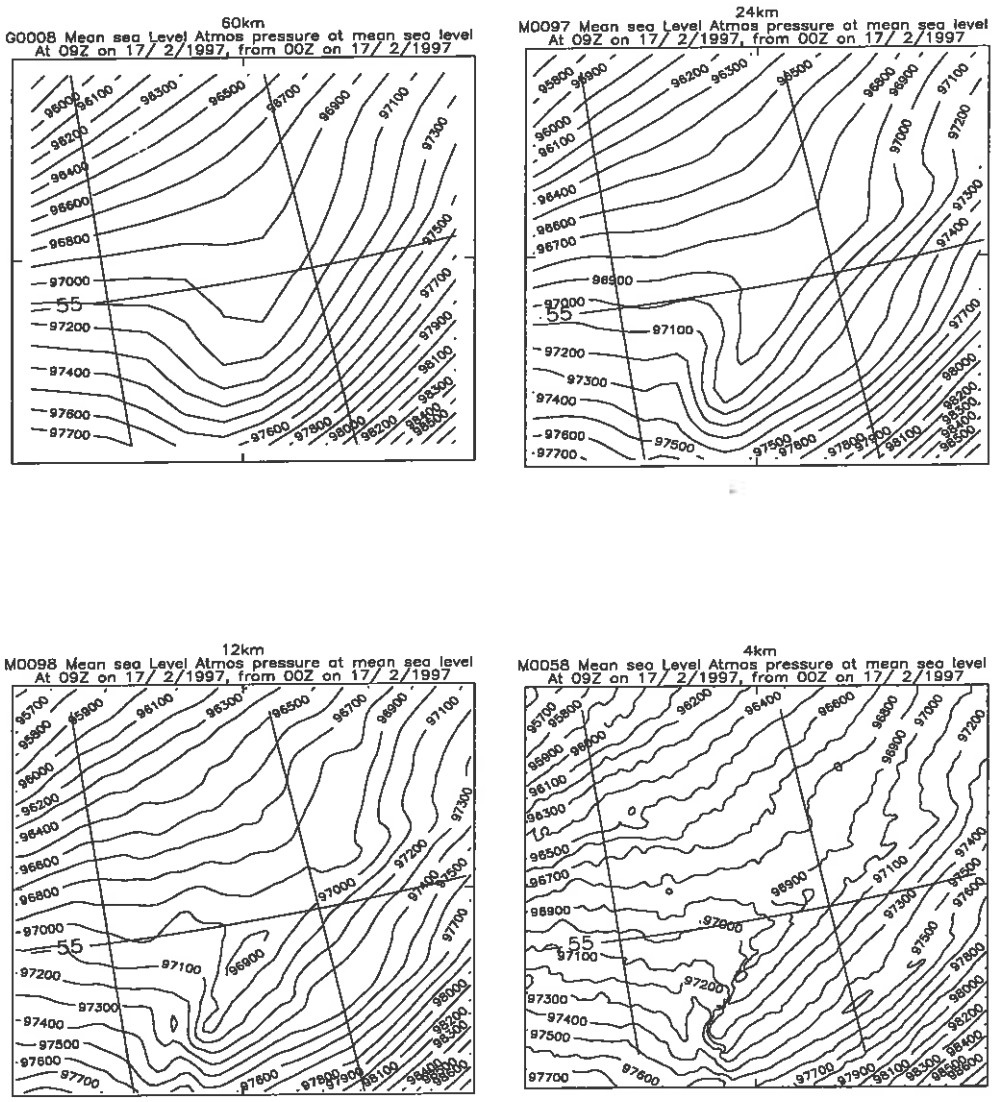

Figure 3.1 pmsl at 9Z (T+9 forecast) for 60,24,12 and 4km runs.

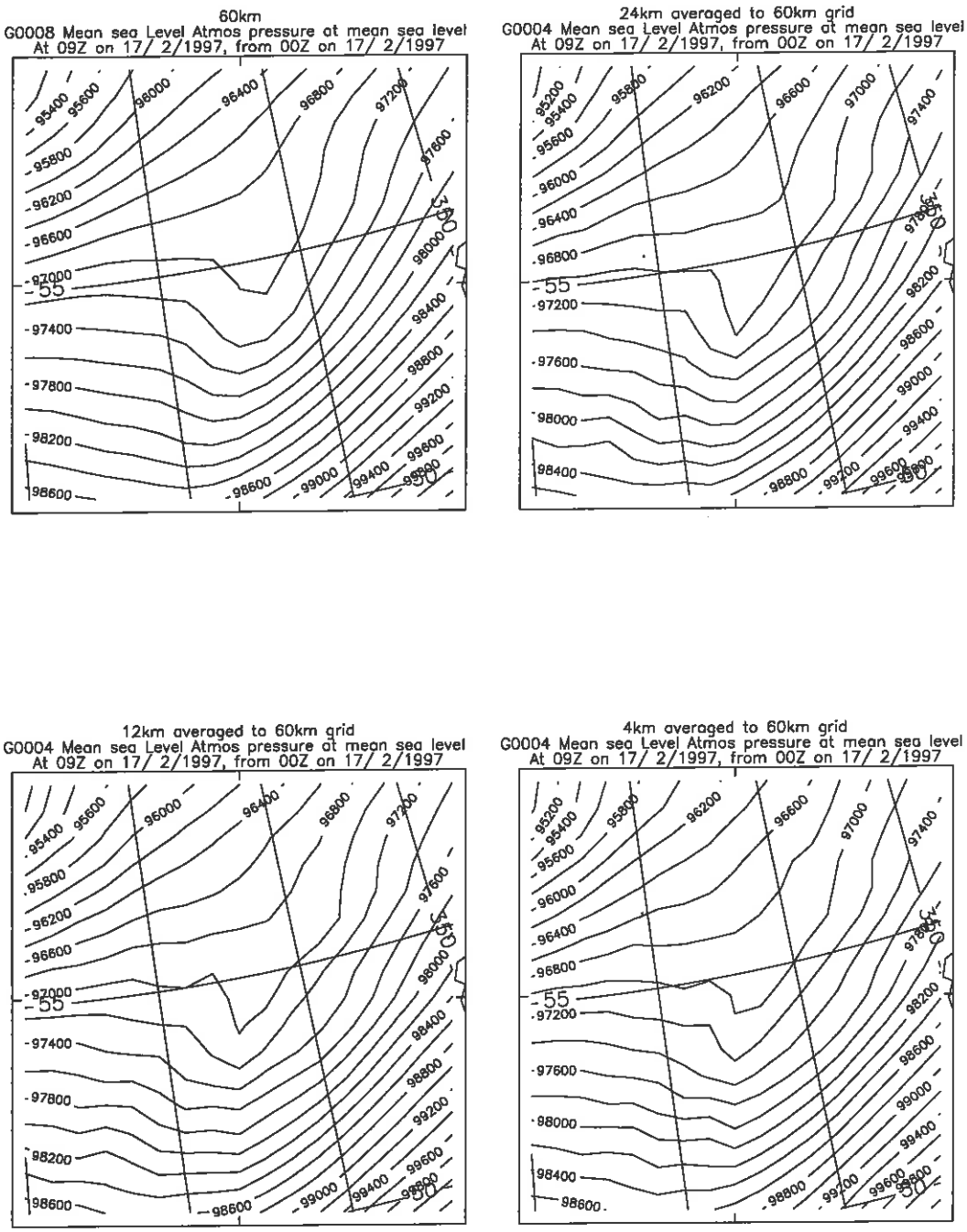

Figure 3.2 pmsl at 9Z (T+9 forecast) for 60km model and higher resolutions averaged to 60km grid.

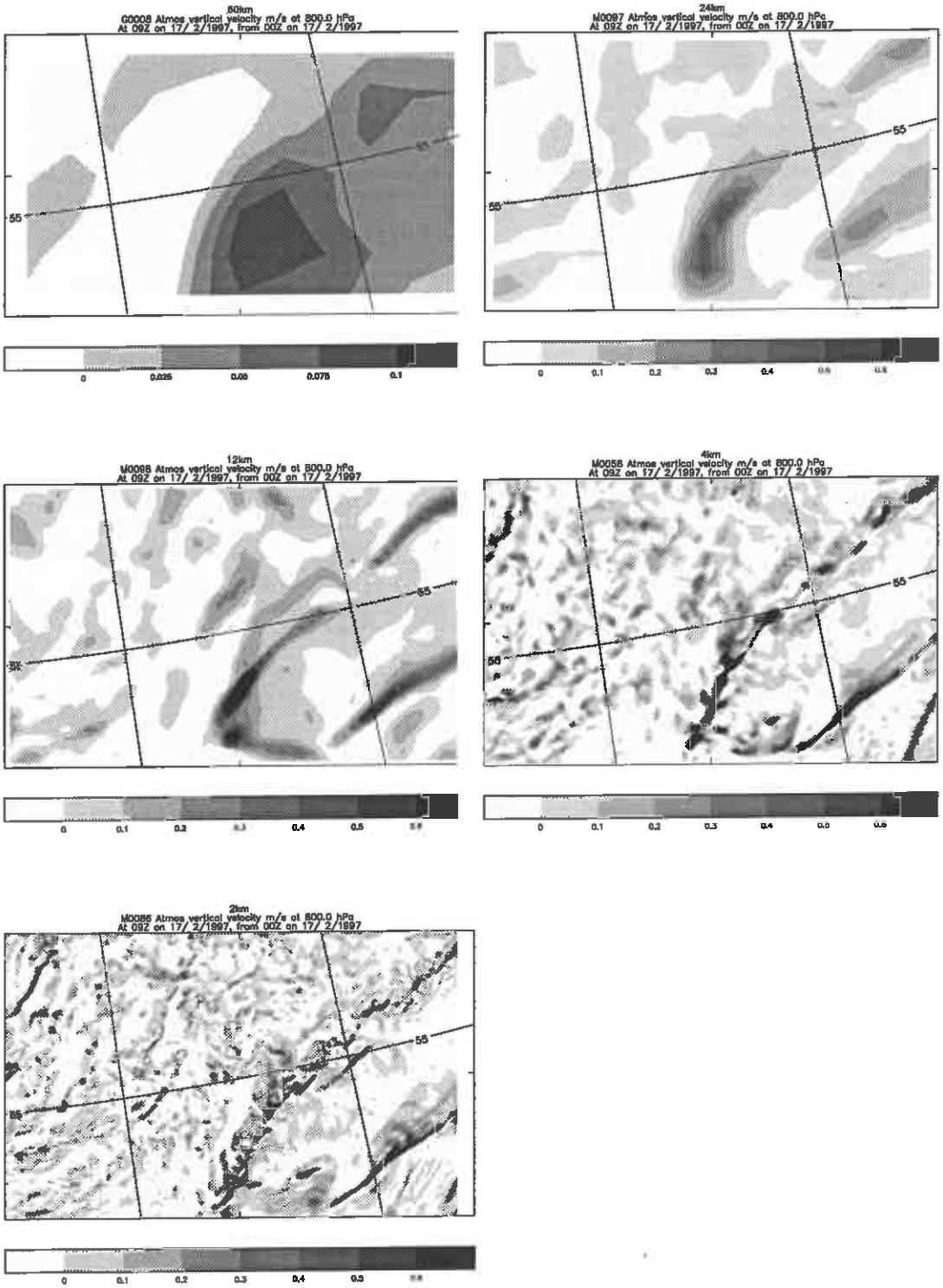

Figure 3.3 800hPa vertical velocity for the various horizontal gridlengths. Note that the scale is different on the 60km model plot. The area shown is roughly the whole area of the 2km model domain.

3. Dynamic Fields at Varying Horizontal Resolution

Figure 3.1 shows a comparison of pmsl for the system at the various horizontal gridlengths. The 60km model fields shown in this report have been interpolated onto a 60km rotated grid with the same pole as that used in the mesoscale runs in order to allow clean comparisons. In all cases checks were made that this process did not degrade the data. The biggest change in the pmsl for the system is seen going from the 60km to the 24km model with the system elongating and the trough extending to the SW becoming sharper. Decreasing the gridlength to 12 and 4km doesn't change the overall structure but introduces more short range structure which appears as waves in the isobars. Although this may appear to be just noise it is noticeable that these waves do not appear to the SE of the system and are associated with the convective like cells behind it. The field for the 2km model is not shown since it is very similar to that for the 4km one. This picture is reinforced if the higher resolution fields are area averaged onto the 60km grid as shown in figure 3.2. The averaging was carried out by interpolating the high resolution fields onto a somewhat denser grid than the one they were on originally. This intermediate grid was chosen so that when it was area averaged up to 60km gridlength the resulting grid coincided with the rotated one used to display the 60km data.

Figure 3.3 shows the 800hPa vertical velocity fields for the various gridlength models. One of the features of interest in this case was the double frontal structure which originates from a double trough in the 50km operational analysis. This double structure can just about be seen in the 60km model (particularly if a larger area is viewed than in the figure). This becomes much clearer in the 24km run. Going from 24 to 12km the fronts sharpen up. At 12km the first signs are seen that the northern front is splitting into two with a weaker one appearing to the north. This becomes more obvious at 4km at which point the front begins to break into segments in the along front direction also. These segments may be related to the banding seen across the cloud head in the IR image (see for example fig 5.1). The 2km run shows these more clearly although there is a worry in this case that the breaking up of the fronts may be due to boundary updating. It is also the case that these features are sensitive to changes in timestep and vertical resolution as discussed in section 6. However there is an approximate one to one correspondence between the front segments seen in the 4 and 2km runs (which have different domains). This implies that they might be attempts to reproduce valid features rather than artefacts of the grids/domains being used.

It is also of interest to look at the same fields averaged up to the 60km grid. This is shown in figure 3.4. Once again there is a big change going from 60km to 24km, the double frontal structure becomes much clearer and the overall magnitudes of the vertical velocities increase. However when the gridlength is decreased beyond that to 12, 4 and 2km the averaged vertical velocities do not appear to change very much. This is shown in figure 3.5 which shows a curve of the average upgoing vertical velocities from the data averaged up to 60km as a function of model horizontal gridlength (i.e. an area average with negative values on the 60km grid squares set to zero). Since we are mostly interested in the representation of the system this calculation was done over the area of the system only (i.e. roughly the right hand half

of the domain shown in fig 3.3). Although the values change by 50% going from 60km to the highest resolutions, most of this change is going from 60 to 24km. At

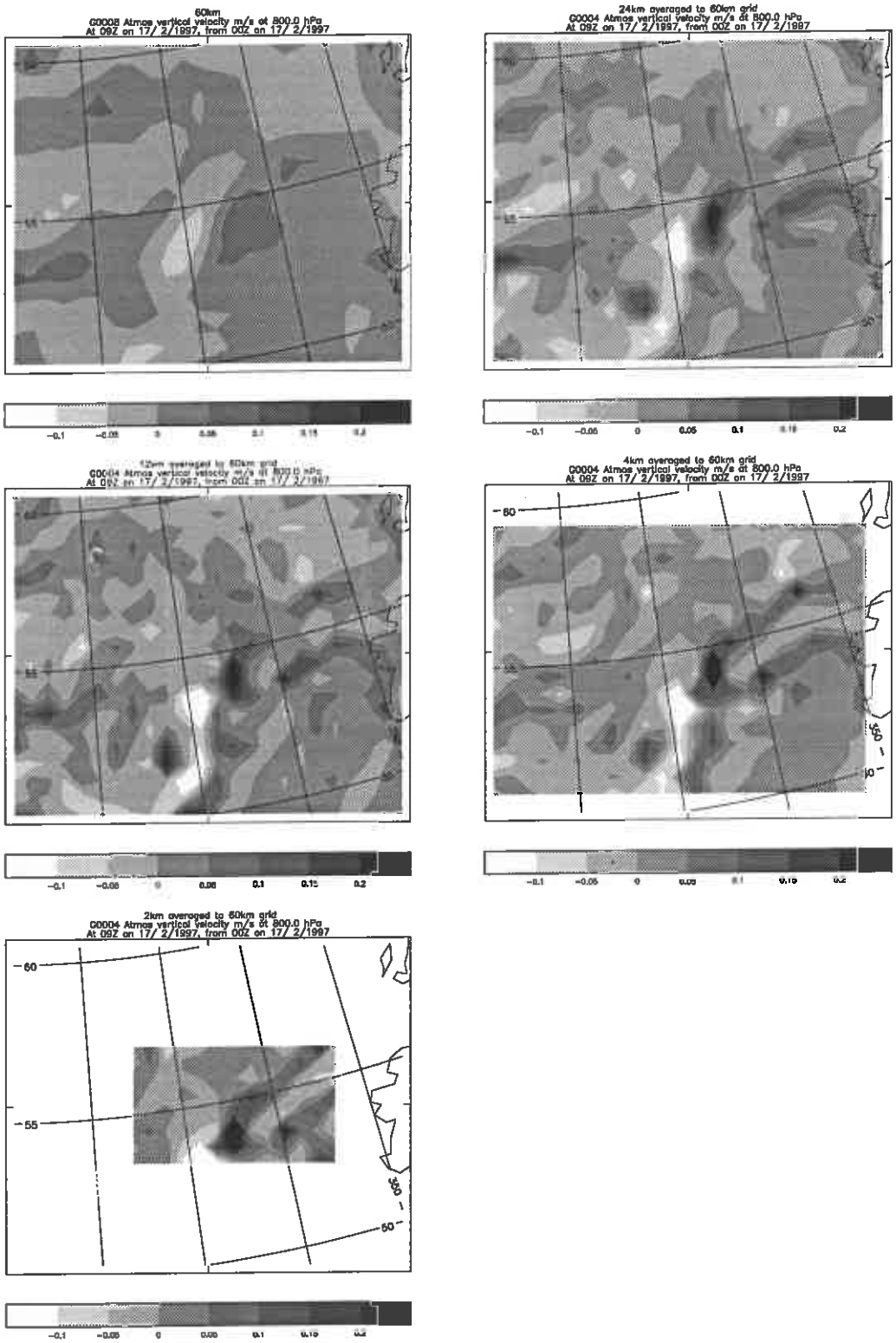

Figure 3.4 800hPa vertical velocity from T+9 forecast averaged to 60km grid.

gridlengths of 12km and below the values change by only a few per cent. This is encouraging in that although the high resolution models produce extra structure at small scales, these structures are consistent with the subgrid parameterisations in the low resolution models.

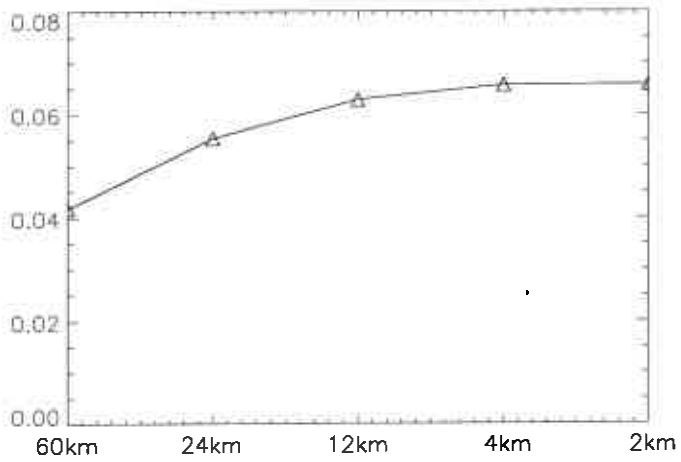

Fig3.5 Average upward vertical velocity for system for different gridlengths averaged to 60km grid

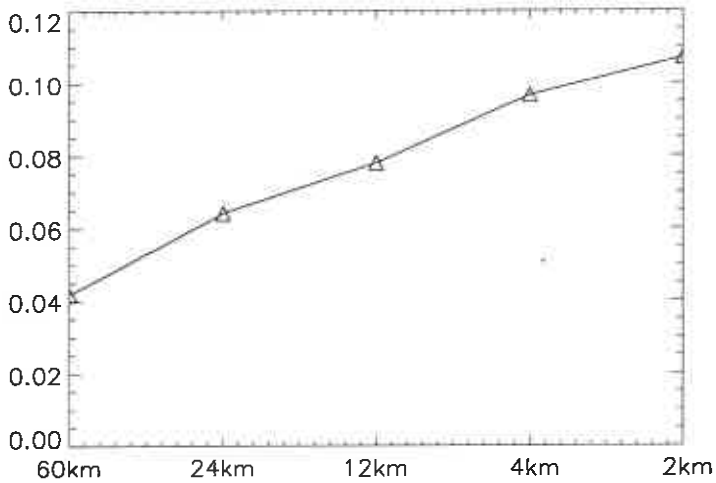

Fig 3.6 Average upward vertical velocity for different gridlengths

In contrast figure 3.6 shows a similar plot of averaged upward vertical velocity but using the data at the model resolution rather than averaged to 60km (i.e. the data on the original model grid was taken and averaged after gridpoints with negative values were set to zero). In this case there is a steady upward trend. This is interpreted as being due to vertical velocity features on scales of less than 60km, i.e. mesoscale structure which cancels out when the averaging to a 60km grid is carried out. Although the detailed curve changes the overall upwards trend is insensitive to the area of the model chosen (i.e. including the system or not) and also to the inclusion of the runs with the convection scheme suppressed. It is shown in Annex A that the curves shown in figs 3.5 and 3.6 are consistent with the models having some knowledge of the subgridscale structure rather than simply aliasing all the subgridscale vertical motion to the gridscale. The work presented below on the energy spectra of the fields shows there is still some aliasing onto the gridscale and a more detailed discussion can be found there.

Figure 3.7 shows an attempt to compare the vertical velocities on one of the fronts at different resolutions. At high resolutions the fronts will be narrower but have a higher peak vertical velocity associated with them. Figure 3.7 shows the total area times 800mb vertical velocities for a 150km length of the northernmost front at 9Z – i.e. a measure of the total upward motion. All values below 0.2 of the peak value at a given resolution are excluded in an attempt to include only motion associated with the front. (This is essentially the same information as figure 3.5 except focussed on the front). The figure shows that the total upward motion varies by almost a factor of two but this variation is somewhat smaller if the 60km run is excluded. Contrary to what might be expected the total upward motion falls off as the gridlength is reduced below 12km. This appears to be a result of the models convection scheme: the dotted points in the figure which represent runs in which the convection scheme was suppressed by using a very long CAPE closure timescale (1000000s) and show the upward motion staying constant as the resolution is increased. The details of this need further work but it would appear likely that the convection scheme becomes more active when more extreme vertical velocities are generated.

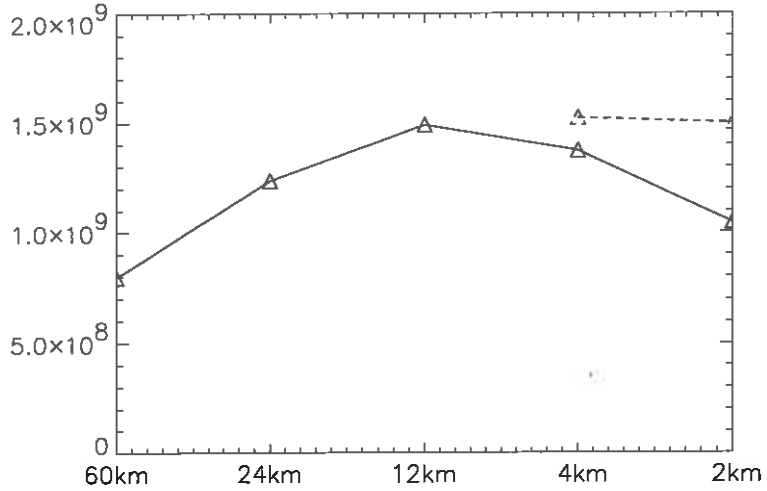

Fig 3.7 Total upwards flux in Northern front for different gridlengths. Solid Lines: Runs with std convection scheme. Dotted line: Runs with convection scheme suppressed.

As mentioned above the 60km model appears to be more different from the 24km than the 24 from the 12 etc. One obvious point of difference is that 60km is the gridlength to which the other models are being averaged. Whereas when the higher resolution modes are averaged to 60km structures would be expected to be observed on this scale, the 60km model itself might be expected to only resolve structures on a scale of 2 gridpoints, i.e. 120km. For this reason a comparison was made between the 60km model and the 24km model averaged to a 120km grid – this is shown in figure 3.8 (along with the 24km averaged to 60km as before for comparison). This figure shows that over most of the domain the 24km averaged to 120km is very similar to the 60km model, much more similar than the 24km averaged to the 60km. This vindicates the view above. However it is also clear that the biggest difference between the 60km model and the 24km averaged to 120km is in the area of the system, it appears as though the system is more strongly developed in the 24km model. In order to clarify the situation further the high resolution fields were also averaged onto the 24km grid and compared to the 24km model as shown in figure 3.9. The argument given above about models only being expected to have an effective resolution of two gridpoints still holds so one would expect the 24km model to look somewhat different (smoother) than the 12km one averaged to 24km. Nevertheless the 12km averaged to 24km looks much more like the 24km model than the 60km model does to 24km averaged to 60. This reinforces the view that the 60km model is more different which is expected from the totals shown in figure 3.5.

Another way to analyse the vertical velocity fields from the models at various horizontal resolutions is to calculate the spectral energy density for the different resolutions. This is shown in figure 3.10. The curves shown in the figure 3.10 were calculated assuming an isotropic distribution i.e. the values have been binned in terms of distance in any direction from the origin in k-space. In order to get a consistent set of curves the fourier transform was carried out on a subset of each grid which corresponded approximately to the area of the 2km grid.

There are two features of these curves worth commenting on. Firstly the cut off at high wavenumbers corresponds to $2\Delta x$ waves (e.g. for the 2km data the cut off at 2.5×10^{-4}m corresponds to a wavelength of 4km). It is immediately noticeable that in all except the 60 and 2km curves there is a turn up as this cut off value is approached. If the curves are regenerated using data over a halved domain not including the fronts (figure 3.11) this turn up is absent implying that the effect is related to the fronts. One might conclude that in the models where the turn up is present the smallest scales due to the line convection at the fronts are being aliased onto the smallest scales in the model. The turn up is presumably not present in the 60km model since it doesn't really capture the fronts at all. More interesting is the lack of the turn up in the 2km model which implies that the model is resolving the scales of the front. Figure 3.12 shows a close up of the northern front in the 800hPa vertical velocity field at 12,4 and 2km gridlength plotted with blocks of shading for each pixel. The figure clearly gives the impression that in the 12 and 4km model the front is collapsing to 1 gridlength wide. This is probably unphysical since the model should not be able to represent

features on scales of less than $2\Delta x$ so it is not surprising that the spectra show signs of aliasing. However when we look at the 2km model the front appears somewhat wider being approximately 2 gridlengths wide. The implication is that, rightly or wrongly, the 2km model is resolving the width of the front. The mechanism which causes this broadening of the front in the model would require further investigation.

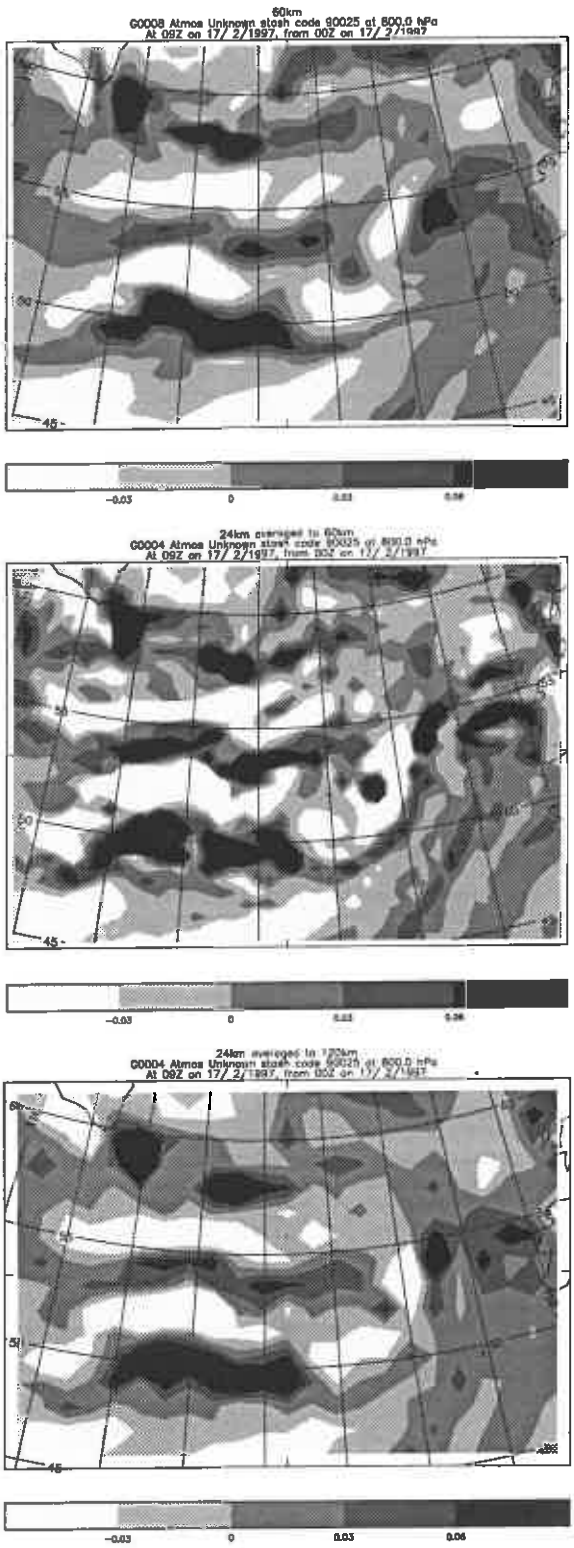

Figure 3.8 800hPa vertical velocity from the 60km model and the 24km model data averaged to 60 and 120km grids.

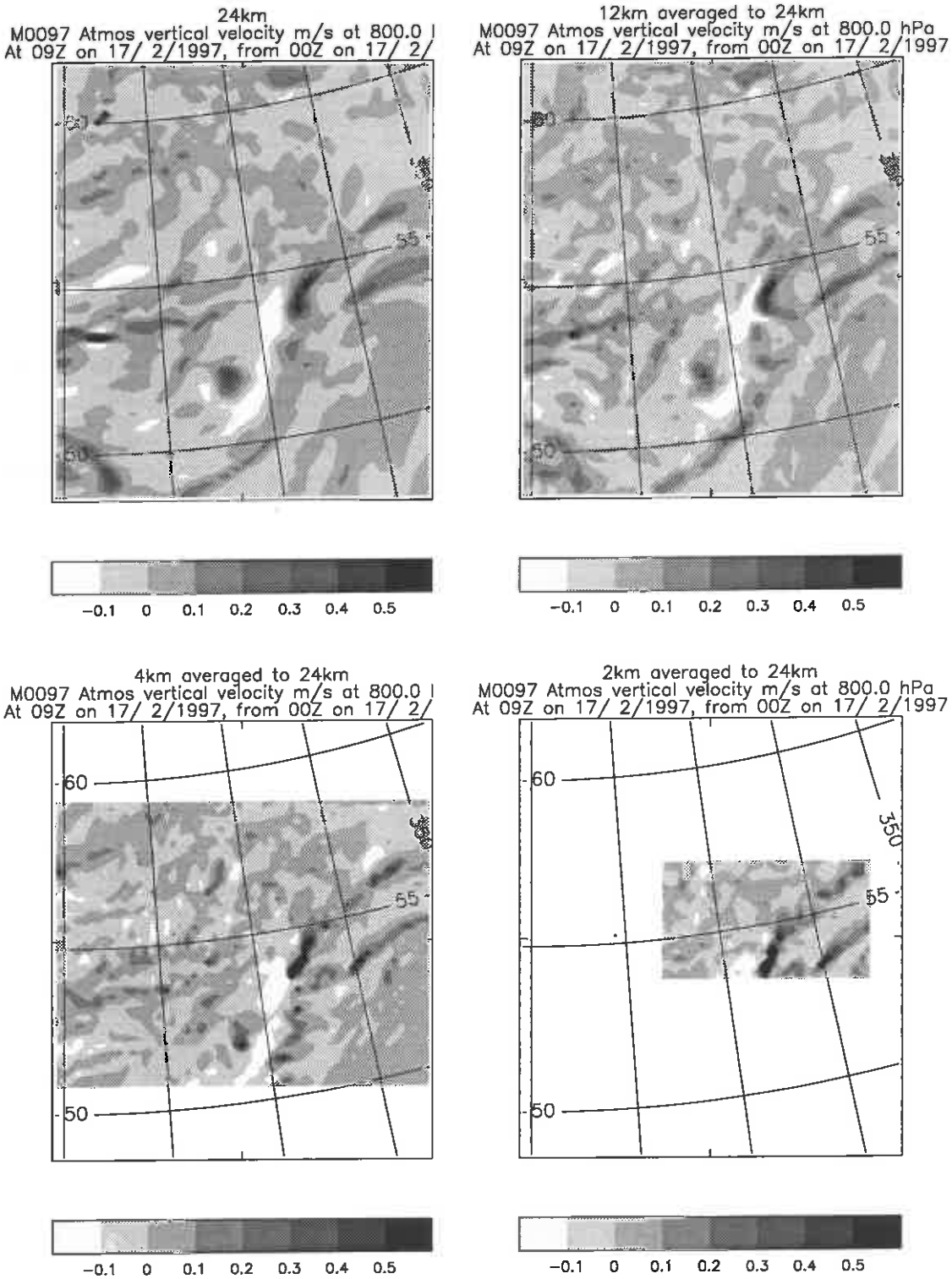

Figure 3.9 800hPa vertical velocity from 24km model and 12,4 and 2km models averaged to 24km.

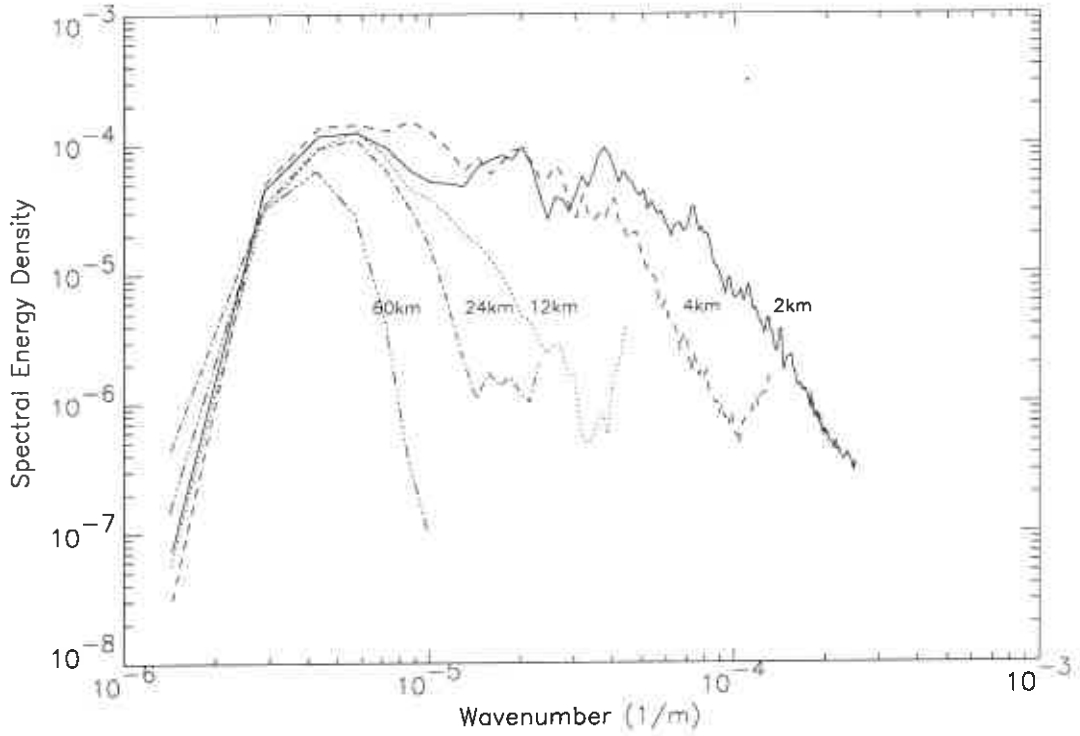

Figure 3.10. Spectral Energy Densities for 800hPa vertical velocity fields at various horizontal gridlengths.

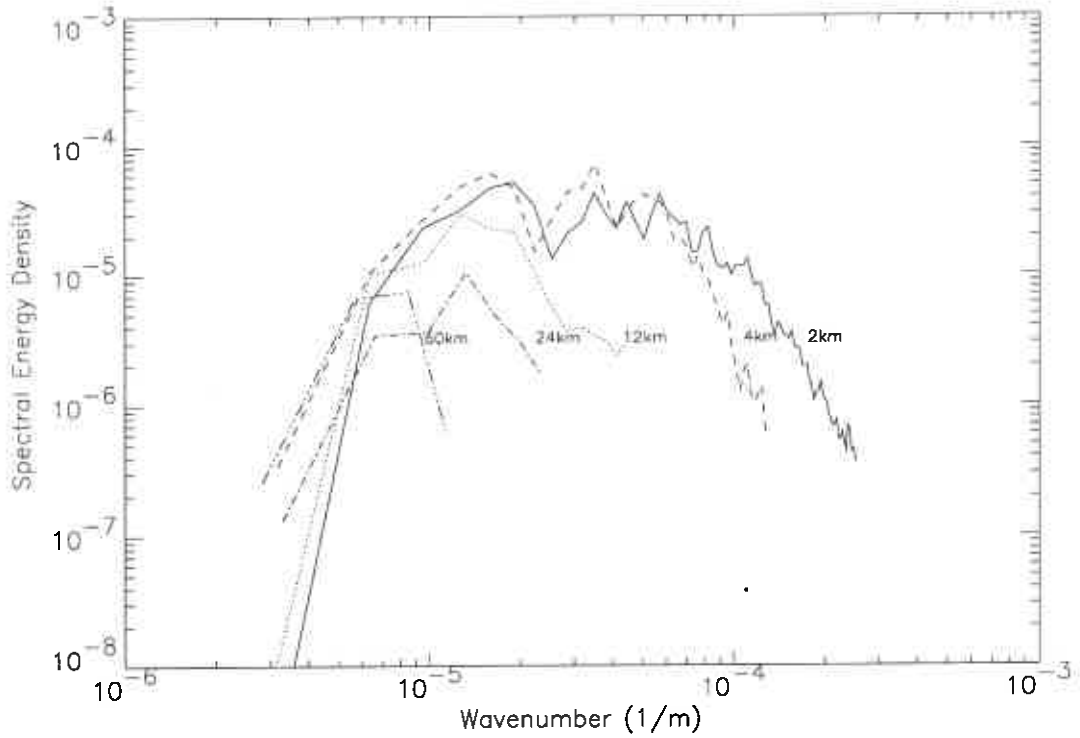

Figure 3.11 As figure 3.10 but for area not including fronts.

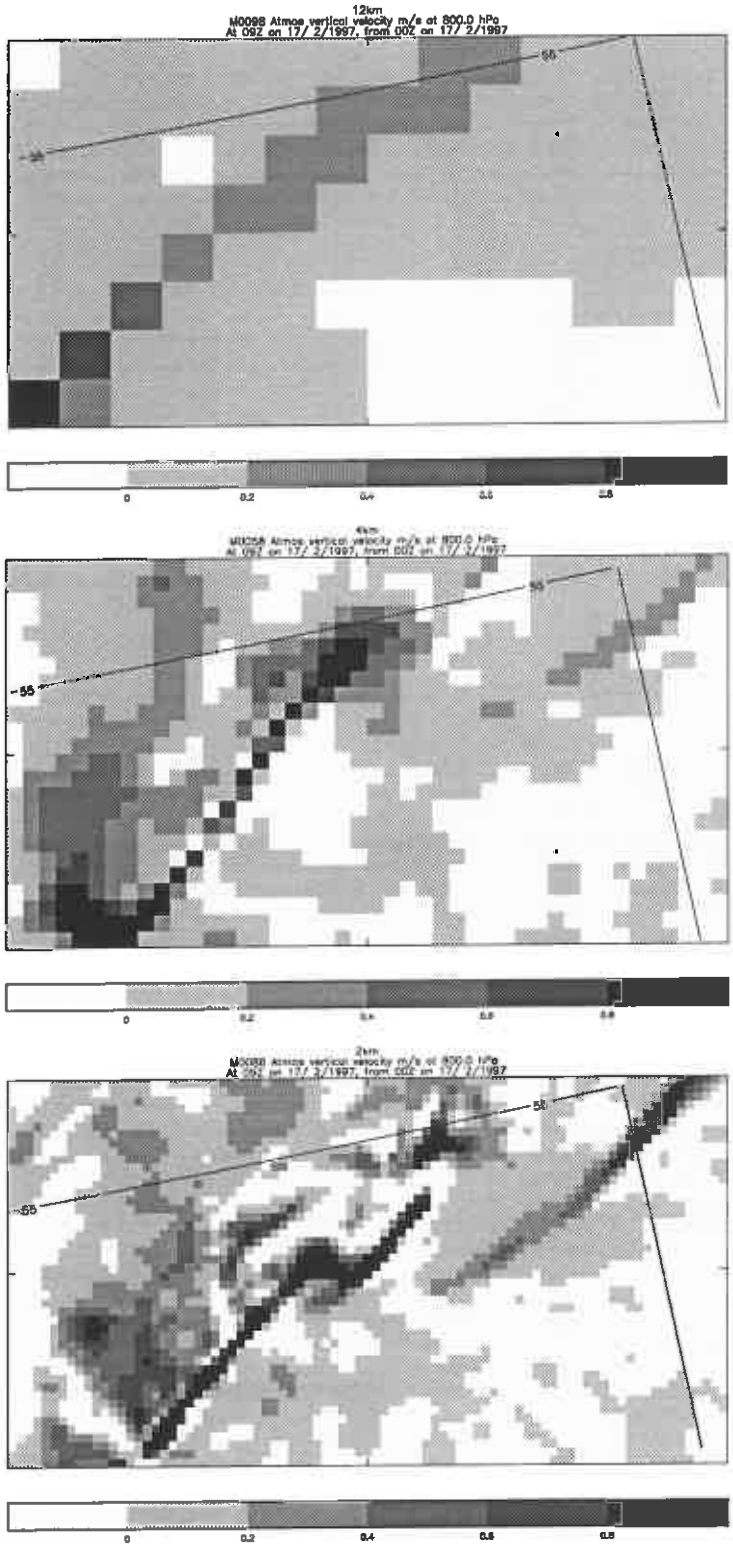

Figure 3.12. Block plot of 800hPa vertical velocity on portion of northern front at 12, 4 and 2km gridlengths.

The conclusion, therefore, is that there is significant aliasing onto the smallest scales in all but the 2km model. It is worth mentioning how this fits in with the conclusions from the discussion on averaging above and in Annex A. The conclusion there was that there is evidence that features on smaller scales than the gridlength are not *just* aliased onto the gridscale in the sense that the upward mass flux appears to correctly take into account the amount of background subsidence in the gridbox. Clearly although this is the case much of the frontal structure at higher resolution is appearing at the gridlength scale in the models.

The second feature of interest in the spectra in figure 3.10 is the way that the curves approach a common value at lower wavenumbers (the cut off at the bottom is clearly due to the size of the 2km domain to which all the datasets were windowed). This is what one would hope for since it implies that any resolution model gives the same results provided that one is interested in scales sufficiently larger than the gridlength. As the gridlength is approached, however, the response falls off. In order to further investigate this the effective filter functions of the models are compared in figure 3.13. In this figure each curve has been divided by the 2km data (which is regarded as "truth" for these purposes). In addition the wavenumber has been normalised according to gridlength so that the x axis is (gridlength/wavelength) and the $2\Delta x$ cut off appears at 0.5 for every model. The resulting curves broadly lay on top of each other implying that there is a universal filter function regardless of model resolution. (For clarity the drop off in the power at the long wavelength end due to the domain size has been cut off several of the curves). In this figure the curves approach a value of 1.0 at an x axis value of about 0.1 which corresponds to a $10\Delta x$ wavelength wave. The conclusion is therefore that any features seen in the model which are smaller than $5\Delta x$ are likely to be affected by the model gridlength.

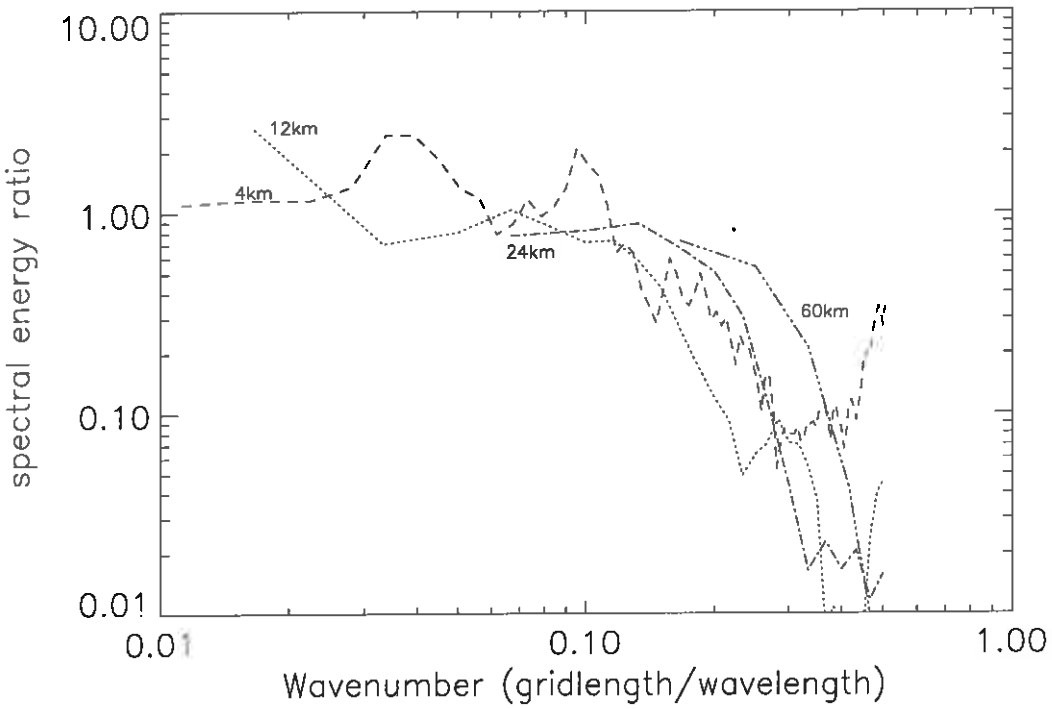

Figure 3.13 Filter functions calculated as described in the text

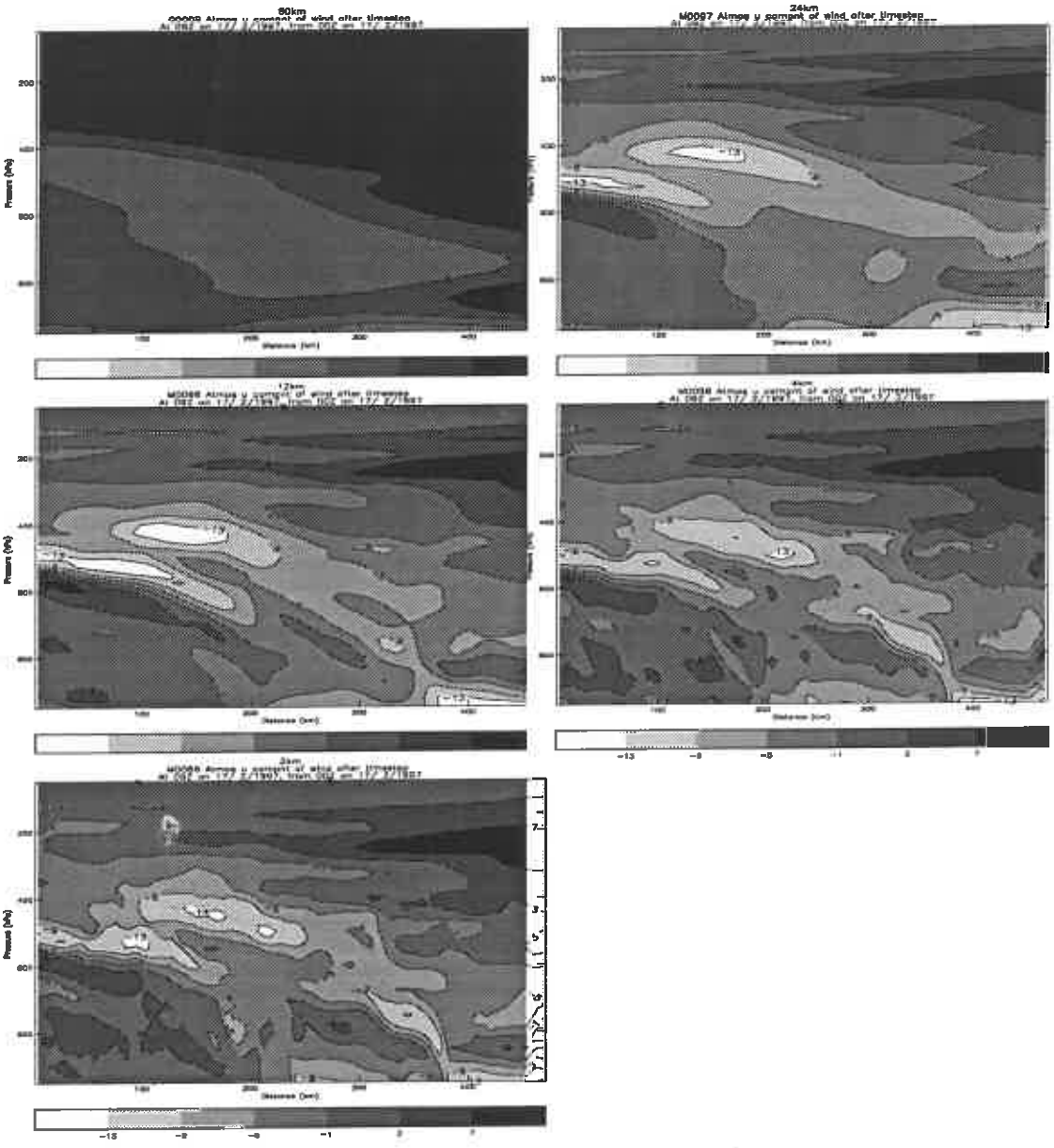

Fig 3.14. Cross frontal velocity cross sections for the various gridlengths. The lighter shadings correspond to velocity towards the cold air (i.e. to the left in the sections).

Turning now to the cross frontal slantwise circulations the cross frontal velocity component is plotted in figure 3.14. As would be expected from the vertical velocity fields all models of 24km resolution and below clearly show a double cross frontal circulation. The circulations do not sharpen up a great deal as the resolution is increased below 12km but this is likely to be related to the fact that the vertical resolution is unchanged across these runs. At resolutions below 12km there are signs that a weaker second circulation is appearing corresponding to the splitting of the northern front mentioned above. This is not clear in figure 3.14 but is shown better in figure 3.15 which is a shorter cross section across just the most northerly surface front at 6Z (when the effect is more pronounced in the part of the model in the domain).

The two slantwise circulations are clearly visible in the 2km run, are somewhat less well defined at 4km and are not present at 12km. As discussed in later sections it is found that the splitting of the circulations becomes much clearer if the vertical resolution of the model is increased.

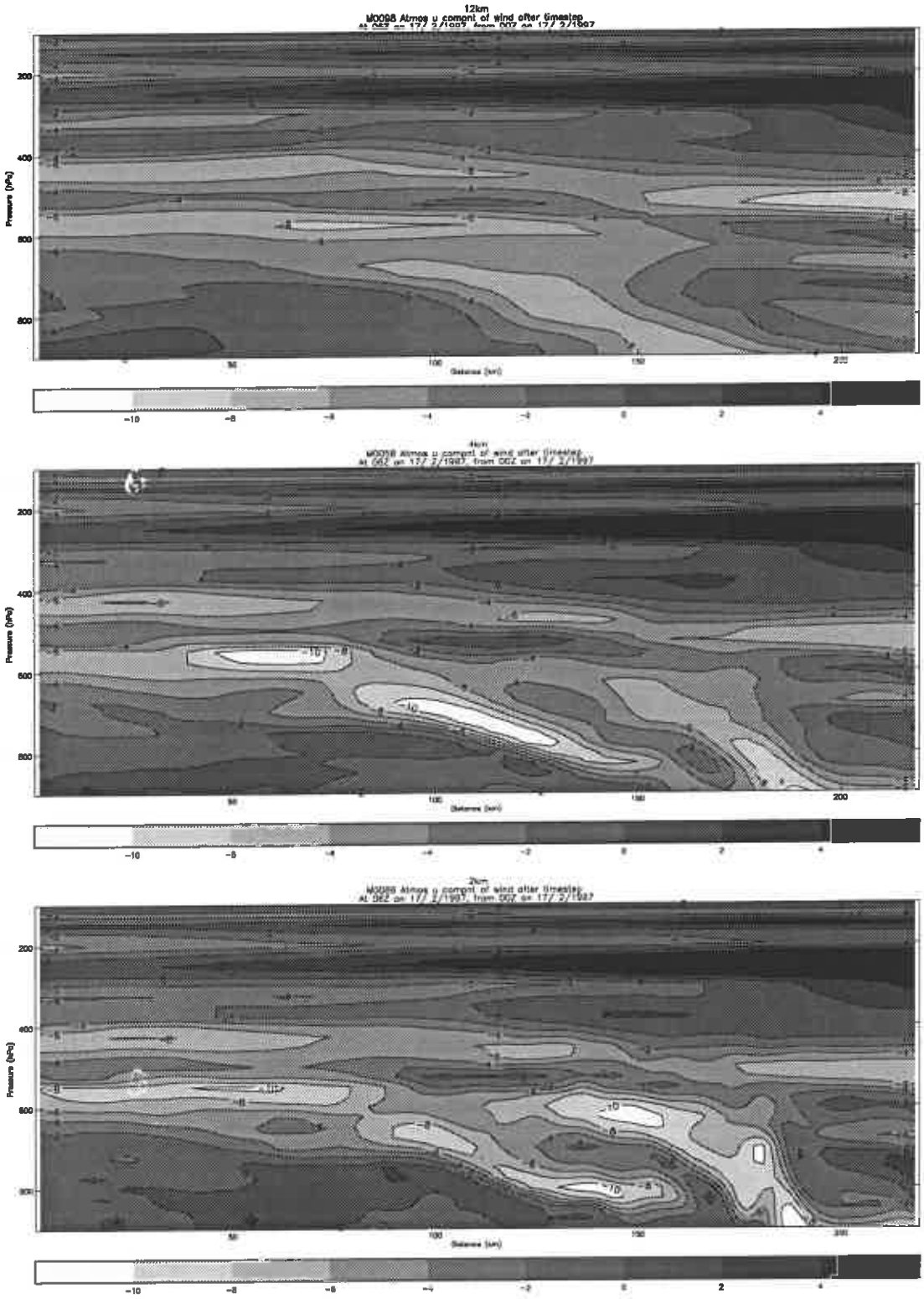

Figure 3.15 Cross Frontal velocity cross sections at 6Z.

4. Microphysical Fields at Varying Horizontal Resolution

This section looks at the resolution dependence of the microphysical fields. The cloud ice fields are shown in plan view in figure 4.1 and in cross section (again across the fronts) in figure 4.2.

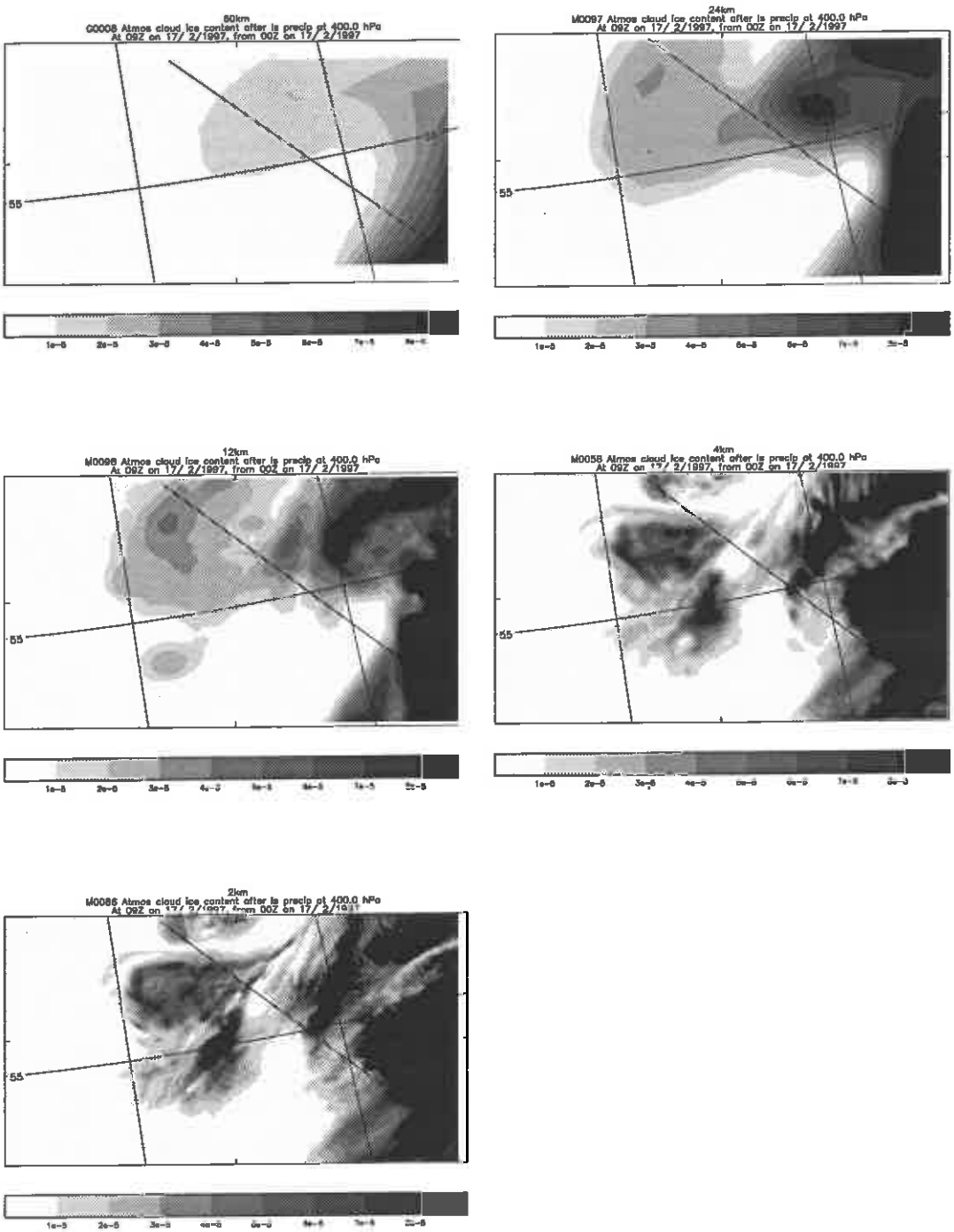

Figure 4.1. 400mb Cloud ice for the various gridlengths.

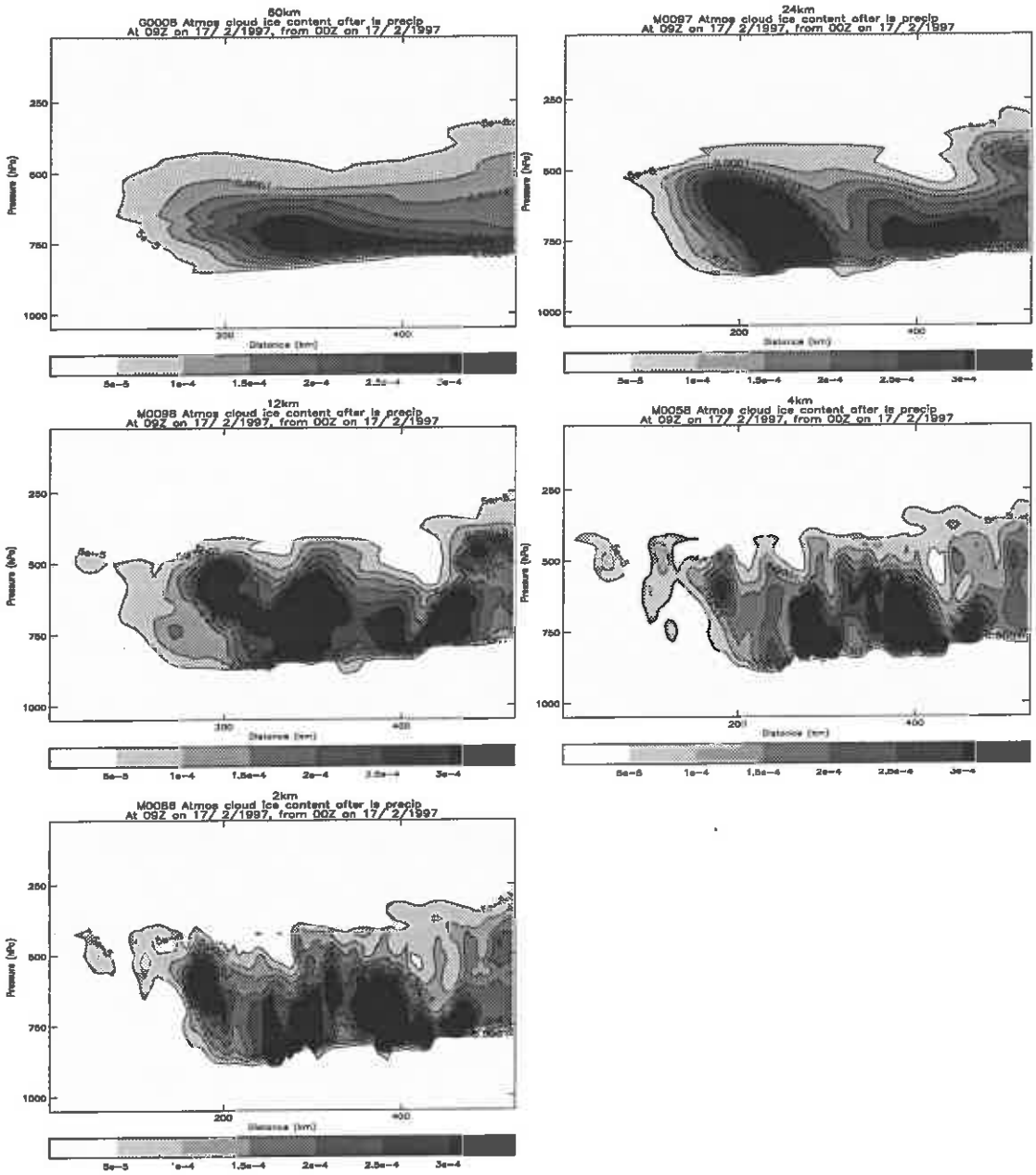

Figure 4.2 Cross sections of cloud ice at positions indicated by line in fig. 4.1

Figure 4.1 shows that again the overall structure is consistent between the models with the cloud shield and part of the cloud head visible. As with the fields discussed in section 3 the biggest change in the 400mb cloud ice field appears to be observed going from 60 to 24km. Consistent with the vertical velocity there are clear signs of the cloud head being split with gridlengths below 24km. At 4km and 2km there are

signs of cross frontal streaks in the cloud heads (see the NW of the domains) which may correspond to the streaks in the cloud head seen in the real system (although again these features are sensitive to timestep and vertical resolution). Figure 4.2 shows vertical cross sections of the same fields – it is clear that many of the same conclusions may be drawn.

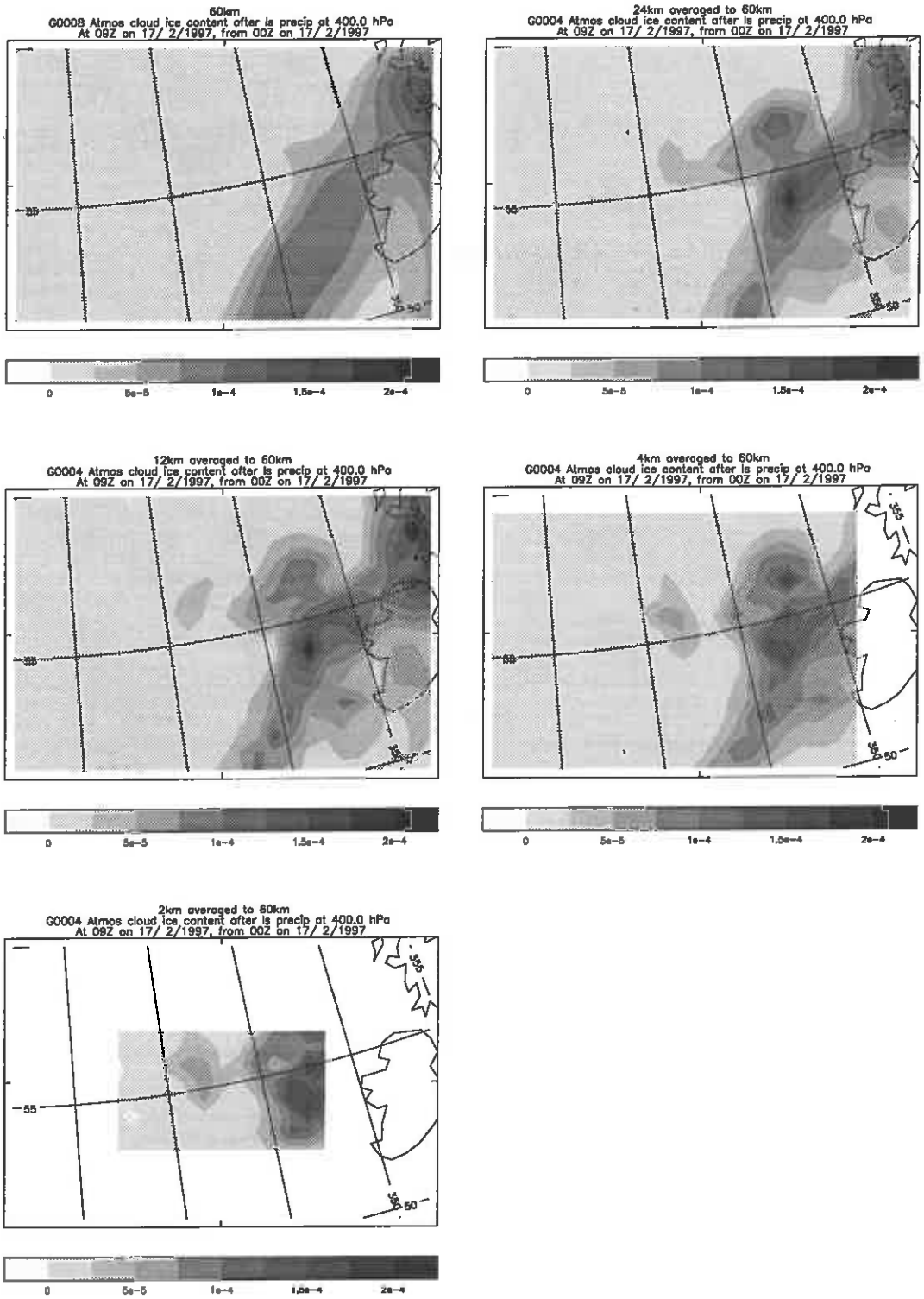

Figure 4.3. 400hPa cloud ice fields averaged to 60km grid for the various gridlengths.

It is instructive to look more quantitatively at the amount of ice in the different models. Figure 4.3 shows the 400mb ice field averaged up to 60km resolution in each case. This figure gives the strong impression that the overall quantity of cloud ice at this level is increasing as the gridlength is reduced. This is confirmed in figure 4.4 which shows the average (taken from the 60k averaged data) cloud ice over a subdomain which covers the system. (approximately the eastern 60% of the 2km domain as shown e.g. in figure 3.3) for both the 400mb and 800mb levels.

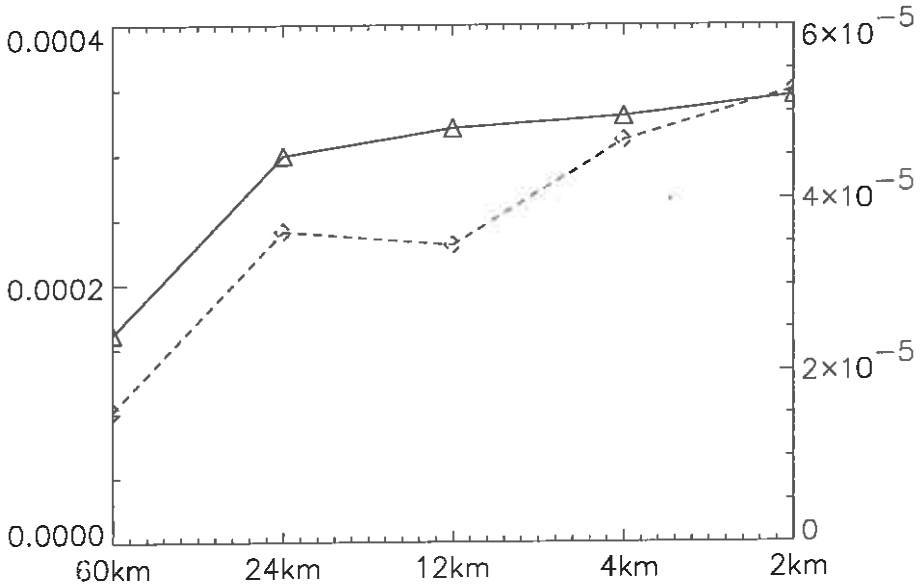

Figure 4.4 Average cloud ice content (g/g) over area of system at 9Z (T+9) at 800mb (sold line, left axis) and 400mb (dotted line, right axis) for various model resolutions.

This confirms that the ice content at both levels increases as the gridlength is reduced. This is more pronounced at 400mb but at 800mb also there is some increase going from 24 to 2km. The increase in ice concentration with reducing gridlength appears to be what would be expected from the trend in mesoscale vertical velocity (see figure 3.6). (The fact that the data averaged to 60km has been used is irrelevant in this case since in contrast to vertical velocity there is no negative ice).

Next the cloud liquid water is considered. Figure 4.5 shows cross sections of the liquid water contents along the same section as shown in figures 4.1 and 4.2. As would be expected there are concentrations of liquid water around the level of the 0°C isotherm. Most of the liquid water above this level is in the regions of slantwise ascent. Figure 4.6 shows a graph of average values of liquid water contents for the different resolutions. The cloud water at 800hPa increases significantly between 24

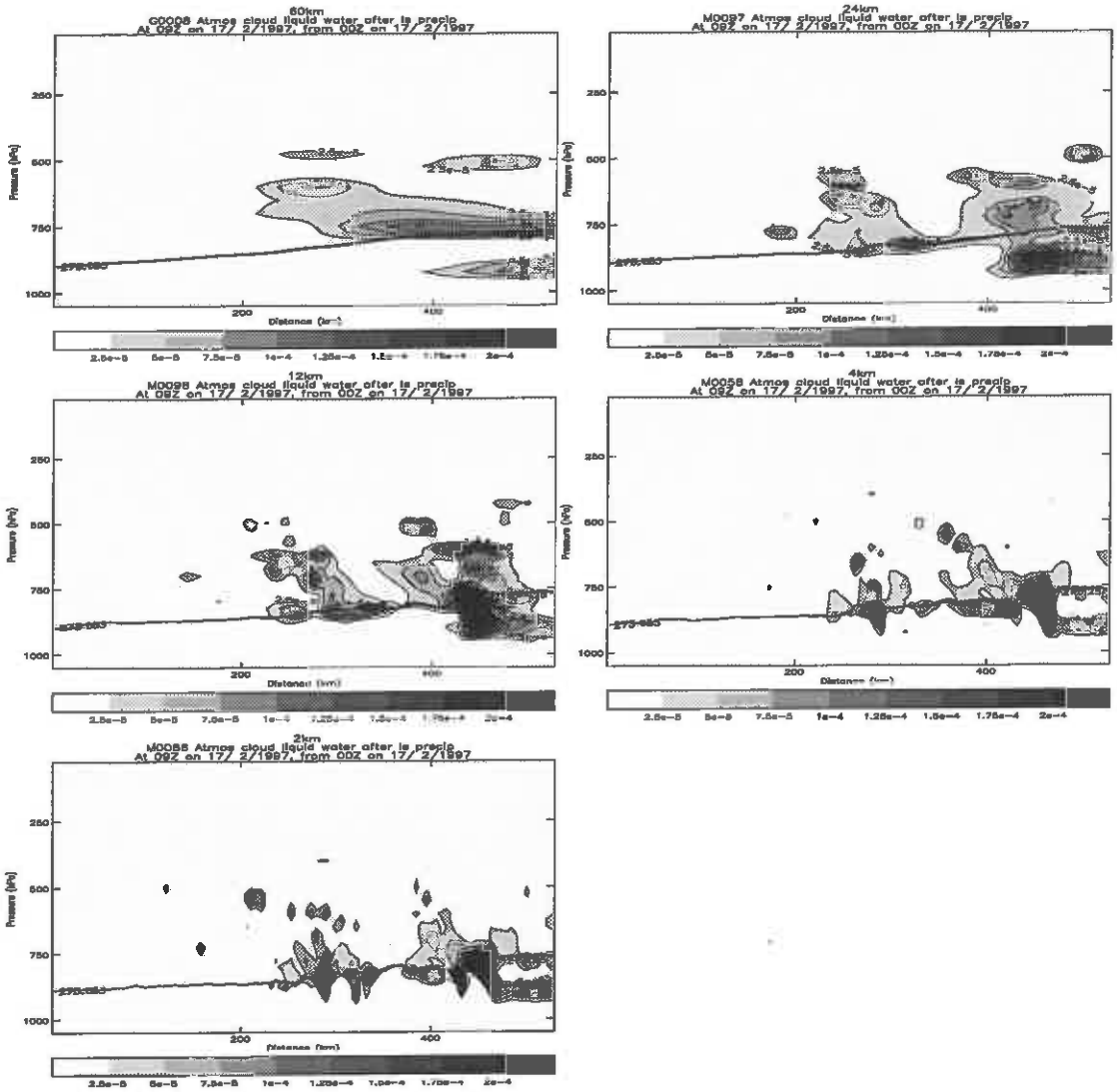

Figure 4.5 Cross sections of cloud liquid water (shading) and 0°C isotherm

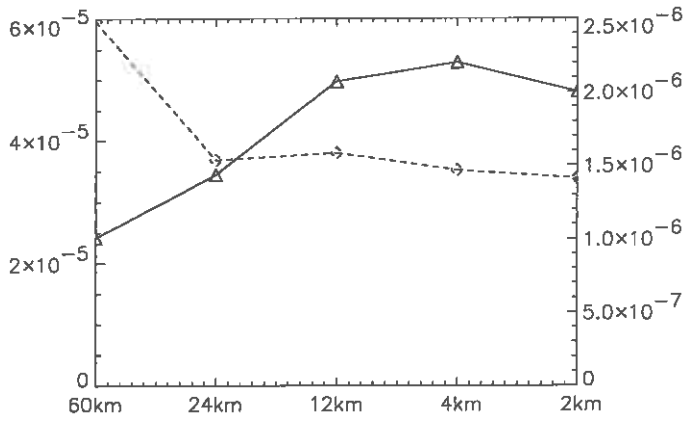

Figure 4.6 Average cloud water content (g/g) over area of system at 9Z (T+9) at 800mb (sold line, left axis) and 400mb (dotted line, right axis) for various model gridlengths.

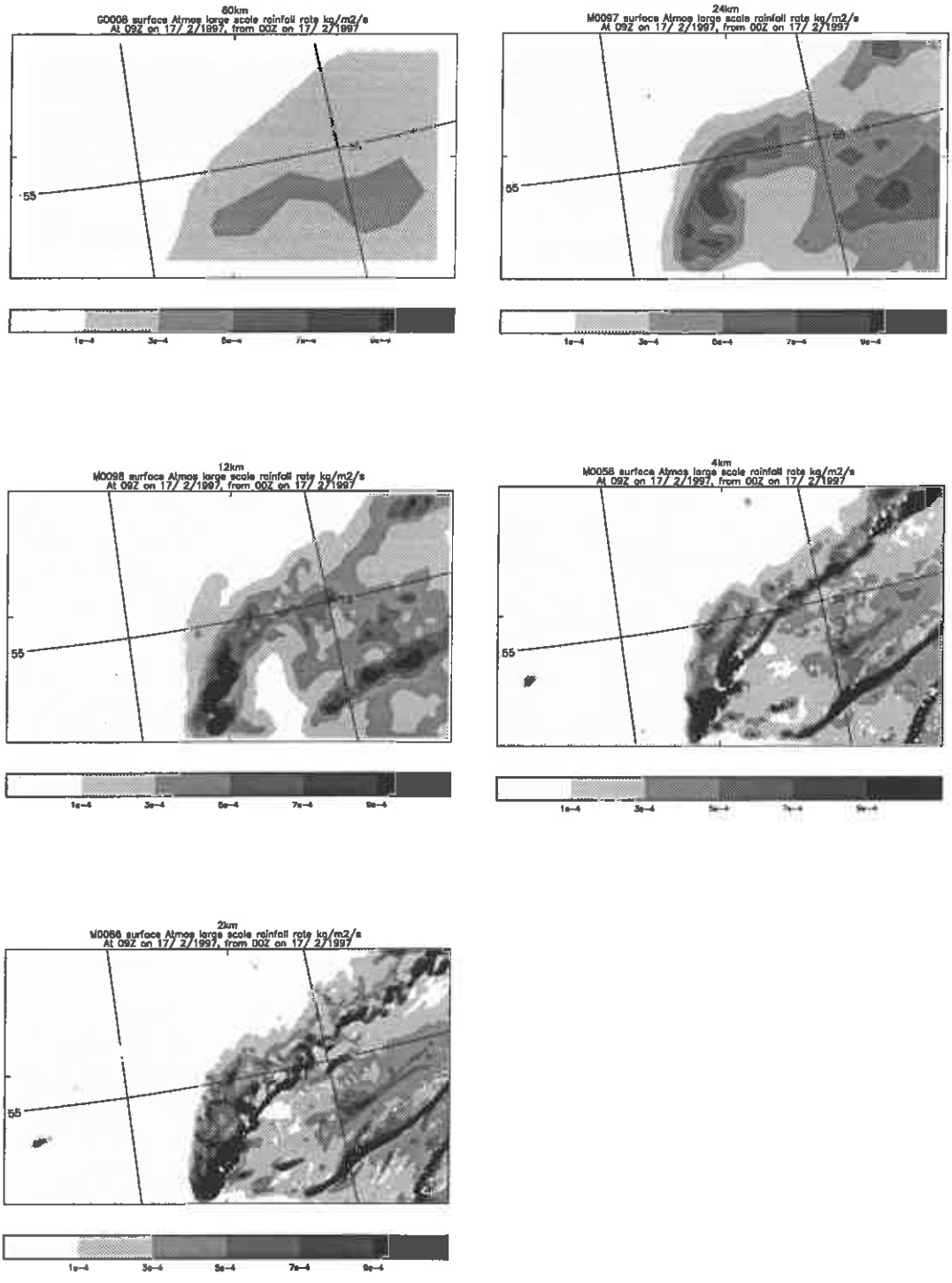

Figure 4.7 Large Scale rain rates for various gridlengths over (approx.) 2km domain

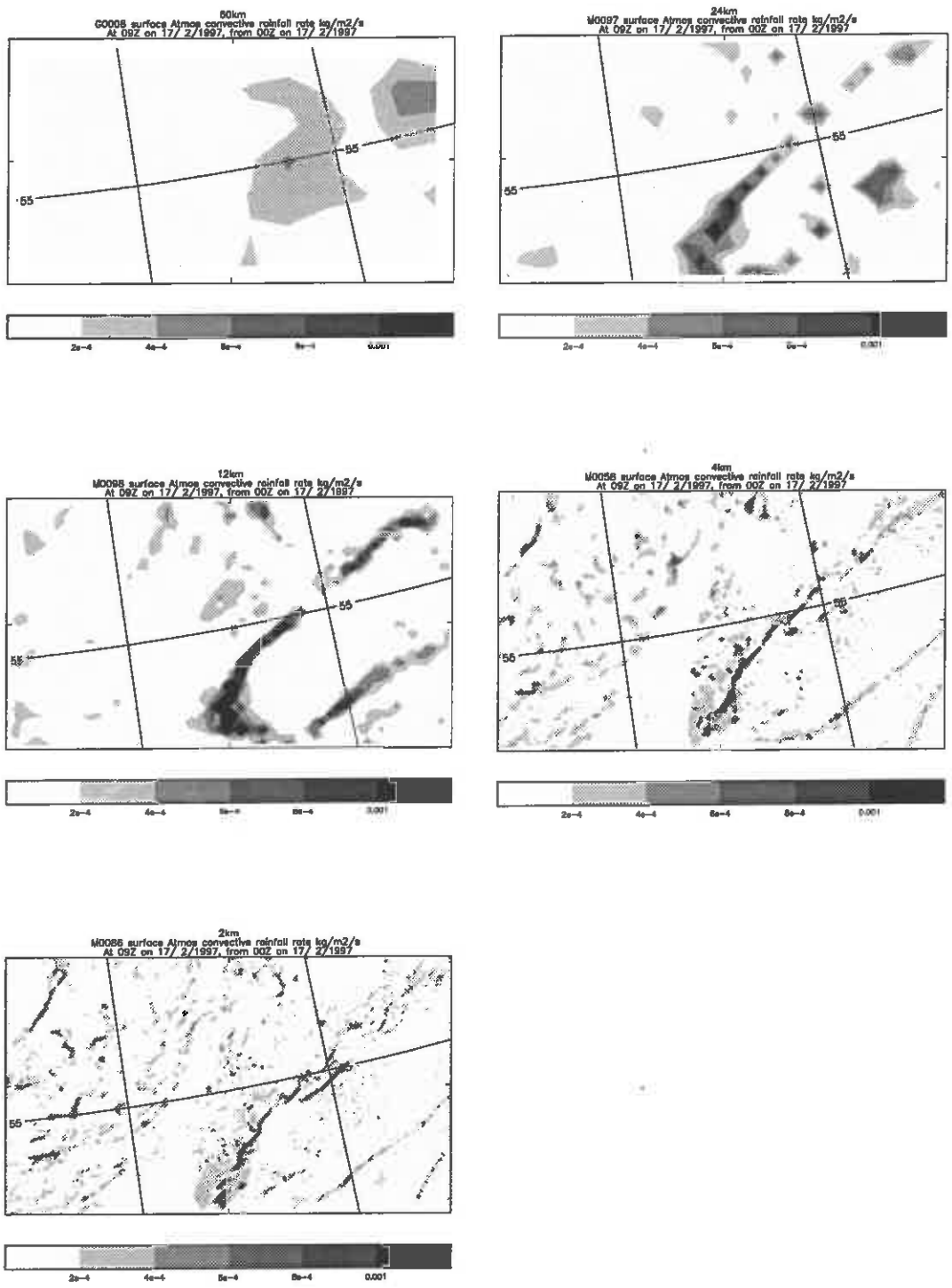

Figure 4.8 Convective Rain rates

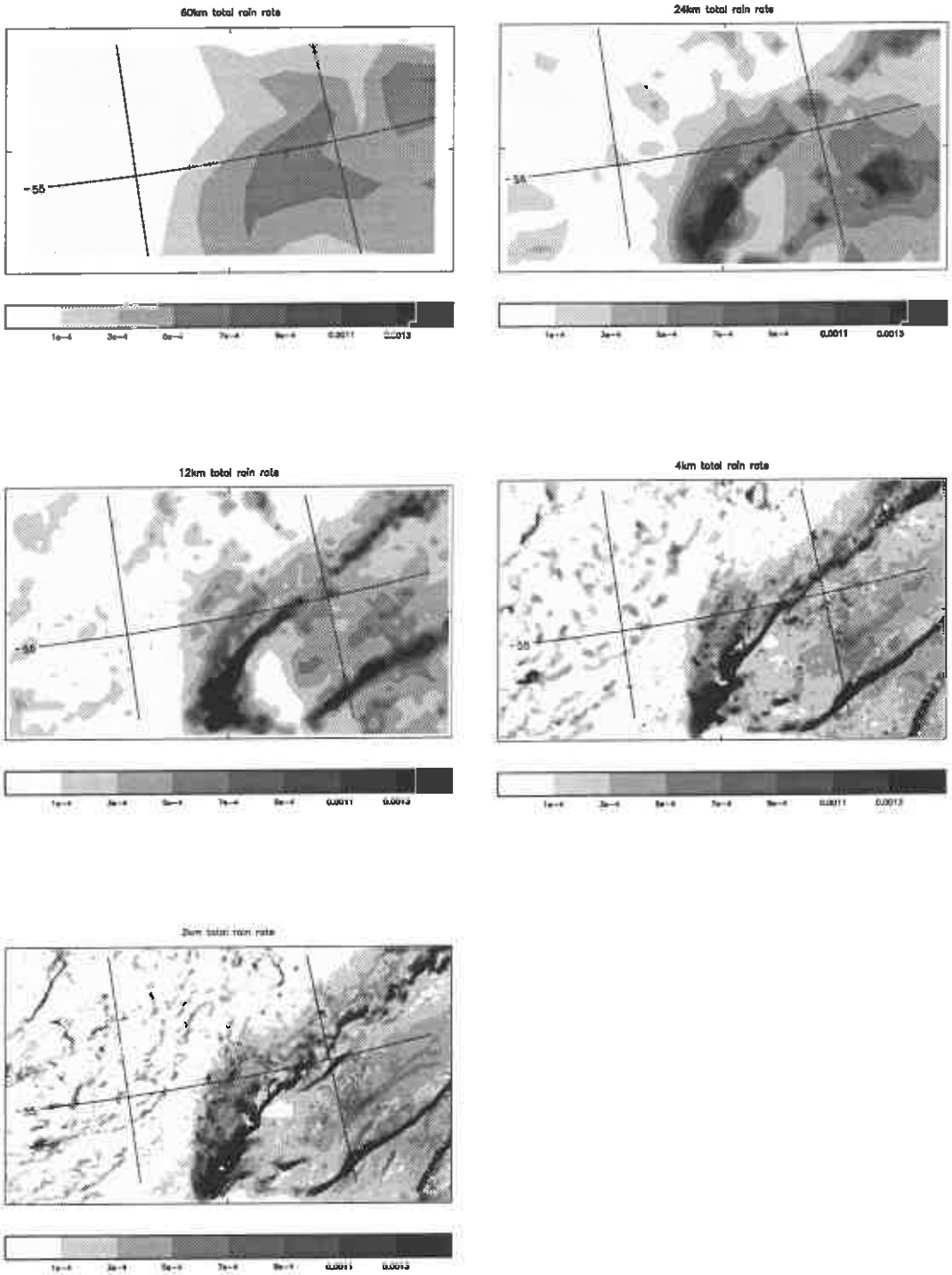

Figure 4.9 Total Rain Rates

and 12km but is roughly unchanged as the gridlength is reduced below this. The water at 400hPa is more constant below 24km gridlength but the absolute water concentrations at this level are very small in any case.

We now consider the rain rates at the various resolutions. Figure 4.7 shows the large scale rain rates for the various resolutions over the domain of the 2km model. Similar features can be seen as in the velocity fields shown earlier, most noticeably the double frontal structure is clearly visible and it is clear that the fronts become sharper as the gridlength is reduced. However it is also immediately clear that the general area and overall intensity of the rainfall does not change much – this is discussed later. Figure 4.8 similarly shows the convective rain rates for the various resolutions. In all cases the models were run with a CAPE closure timescale of 20 minutes (it might well be that, in practice, it is desirable to change the CAPE closure timescale with resolution but it was held constant in this study for clean comparisons). It is apparent that there are many differences between the different resolutions. In all cases (except the 60km) the fronts are marked out as regions of high convective rain rate. Again the scales of features reduce as the gridlength reduces. This is particularly noticeable in the convective region behind the system. The total rain rate resulting from these two contributions is shown in figure 4.9.

Figures 4.10,4.11 and 4.12 show the corresponding rain rate fields averaged to the 60km grid and the average rain rates over the area of the system are graphed as a function of gridlength in figure 4.13. As would be expected the general trend is that as the gridlength is reduced the convective rain rate reduces and the large scale contribution increases. The total rain rate stays constant to within a few per cent as the gridlength is reduced from 24 to 2km which could be taken as a sign that the convection scheme is parametersing the subgridscale processes well. This conclusion should not be expected to be generally true, however, since a more severe test would be a case where the precipitation was dominated by convection. The distribution of the 60km averaged total rainfall (figure 4.12) is also relatively unchanged as the gridlength is reduced from 24 to 2km. This is encouraging since, obviously, the distributions of the large scale and convective rain which make up the total (figs 4.10 and 4.11) individually change more with resolution. Also included in figure 4.13 is the average rain rate for 4km and 2km runs in which the convection has been suppressed by drastically increasing the CAPE closure time. In these runs the large scale rainfall rate is encouragingly close to the total from the runs with the convection scheme operating normally.

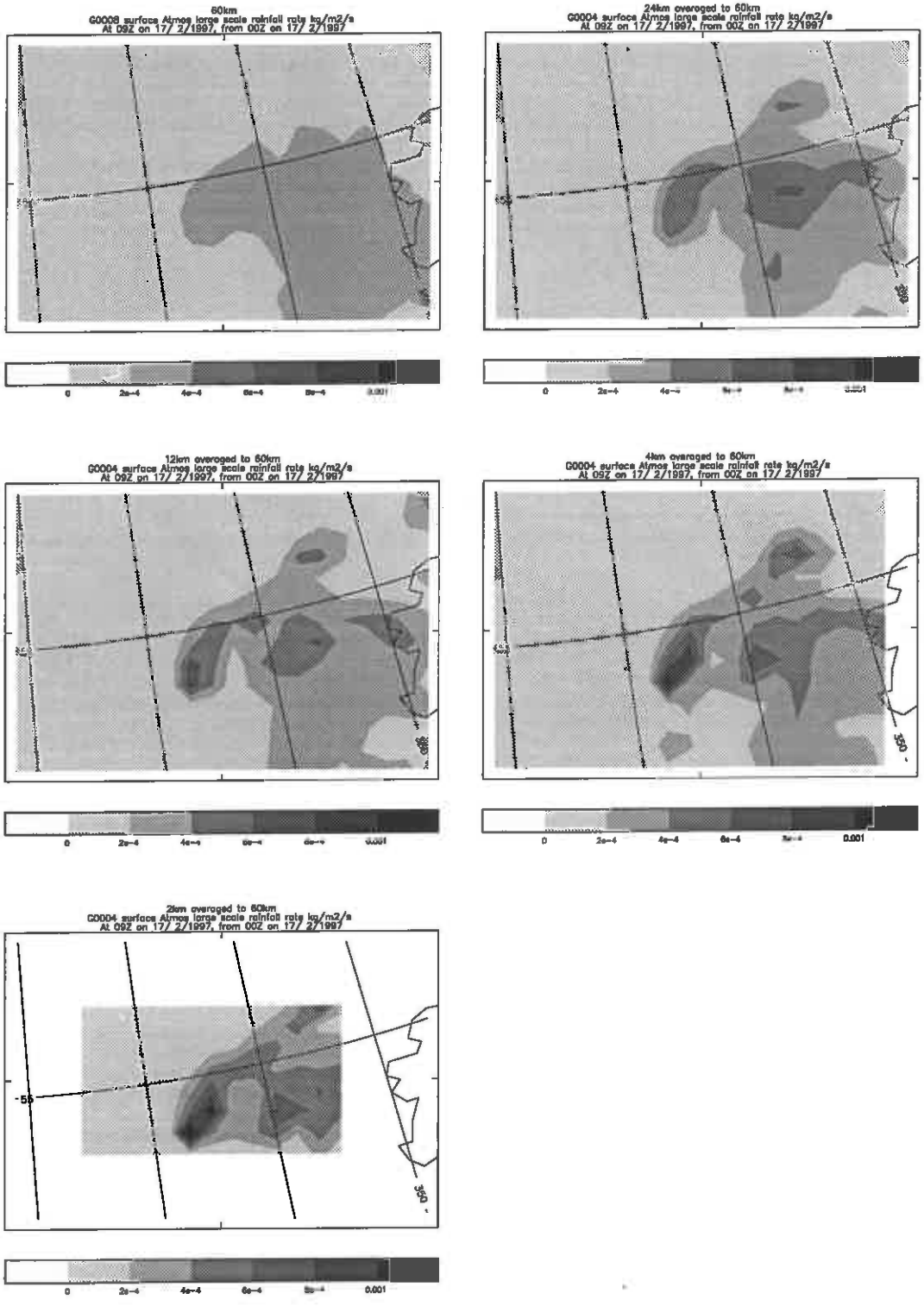

Figure 4.10 Large scale rainfall rates averaged to 60km grid

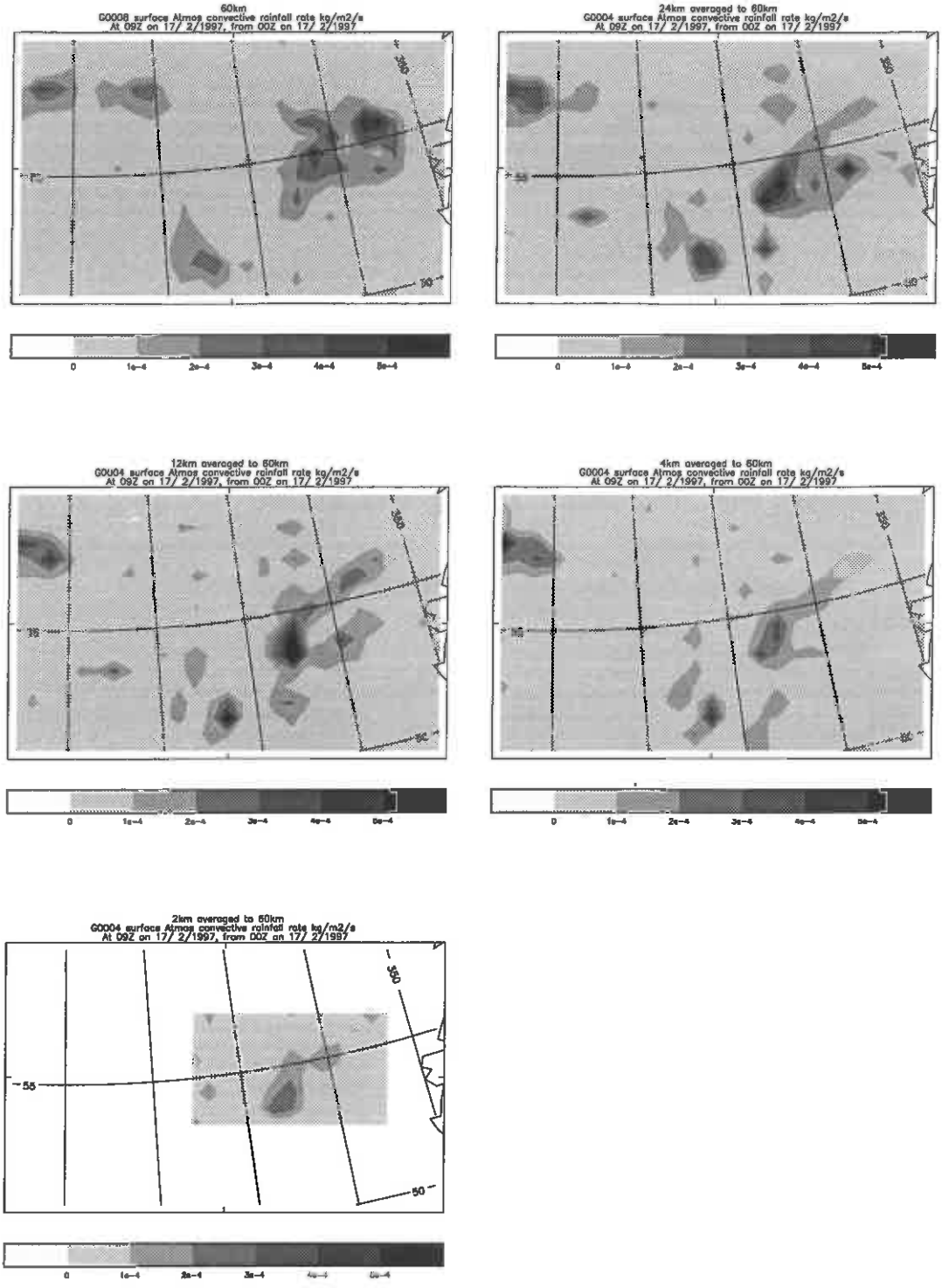

Figure 4.11 Convective rainfall rates averaged to 60km grid

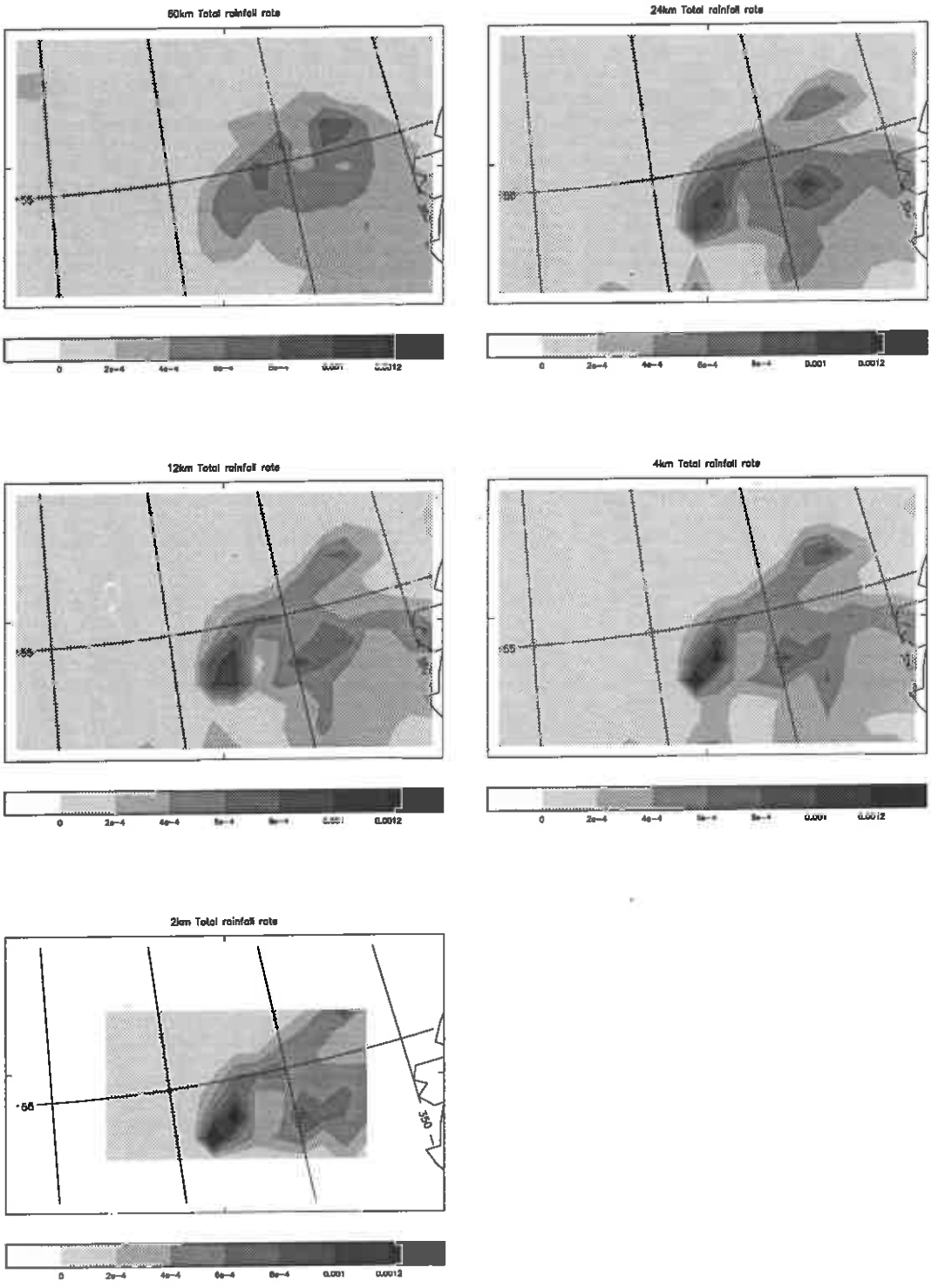

Figure 4.12 Total rainfall rates averaged to 60km grid

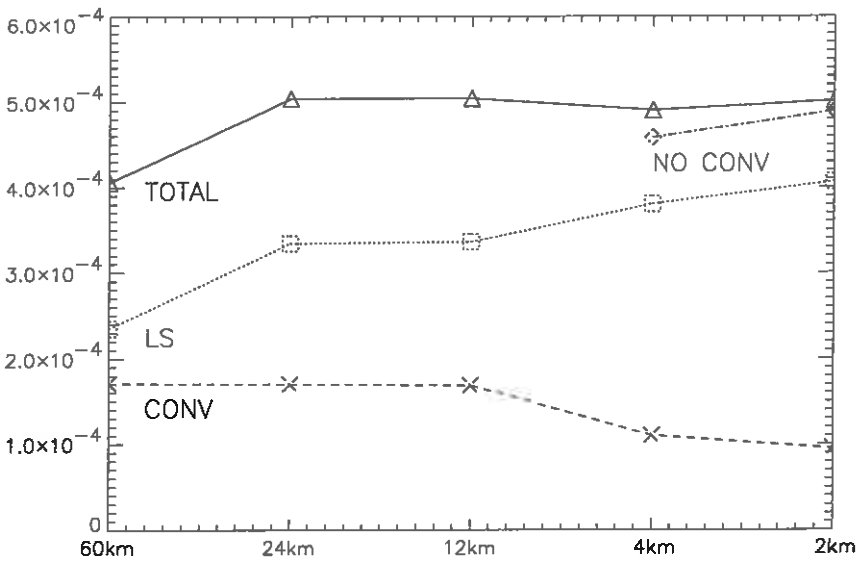

Figure 4.13 Average Rainfall Rates for different gridlengths.

5. Comparison of Various Horizontal Resolutions to Observations

Having presented various effects of varying the horizontal resolution of the model it is natural to ask how well the models verify against observations and if there is any evidence that increasing the resolution leads to a better representation. It is surprisingly difficult to answer this. As discussed by Lean (2000) the FASTEX dropsonde data turns out not to be much help due to poor spatial resolution. The only types of observation discussed here are satellite imagery and radar.

5.1 Satellite Imagery

Figure 5.1 shows the cloud top temperatures for the models of varying horizontal resolution and the IR image. These cloud top temperatures were calculated simply by searching down the model for the first occurrence of a threshold ice concentration. There are obviously gross errors in all the model when compared to observations, for example the cloud heads are overdeveloped. The increasing horizontal resolution, however, does lead to a better representation in the sense that the overall variability of the cloud top temperature looks more realistic. Also as the resolution is increased there is more sign of the uncloudy strip in the cloud shield (towards the bottom right corner of the domain).

5.2 P-3 Radar

As discussed in Lean (2000) we can attempt to compare the models to data obtained by the radar data obtained by the P-3 aircraft. This is shown in figure 5.2 Once again the models are more different from the observations than from each other. All the models appear to be producing too much ice. As with the satellite imagery the main source of encouragement is that the scales of variability look more realistic in the higher resolution models. In this case it is even less clear that there is any benefit in going from 4km to 2km.

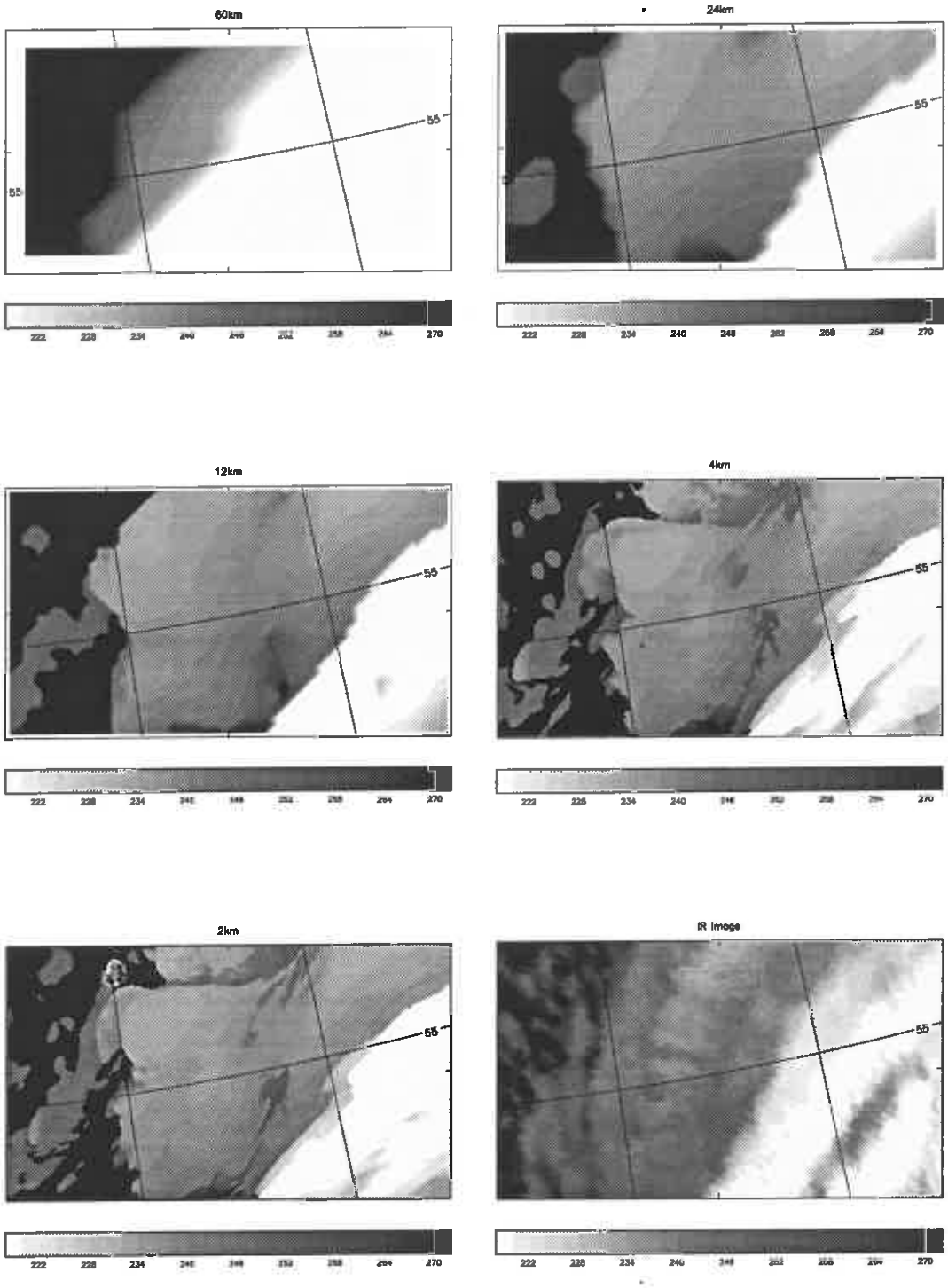

Figure 5.1. Cloud top temperatures for the various horizontal gridlengths and IR image.

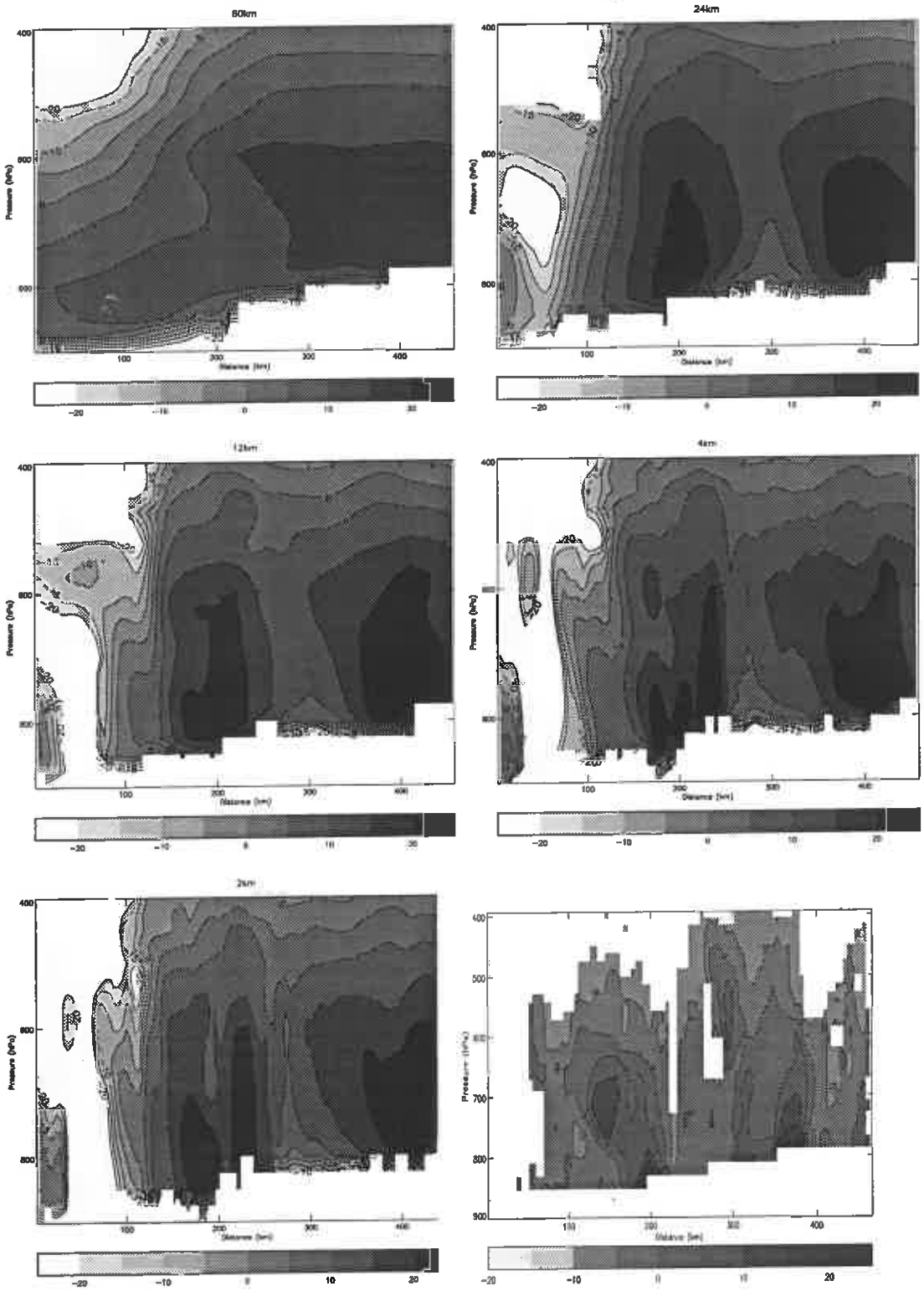

Figure 5.2 Model simulated reflectivities for various gridlengths compared to radar cross section (bottom right).

6. Overview of comparison of models with different vertical resolution.

6.1 4km Model

In this section we look at the effect of vertical resolution in the 4km model. We start with an overview of the effect of using 90 levels as opposed to 45. Figure 6.1 shows a comparison of pmsl between the 45 level and 90 level models.

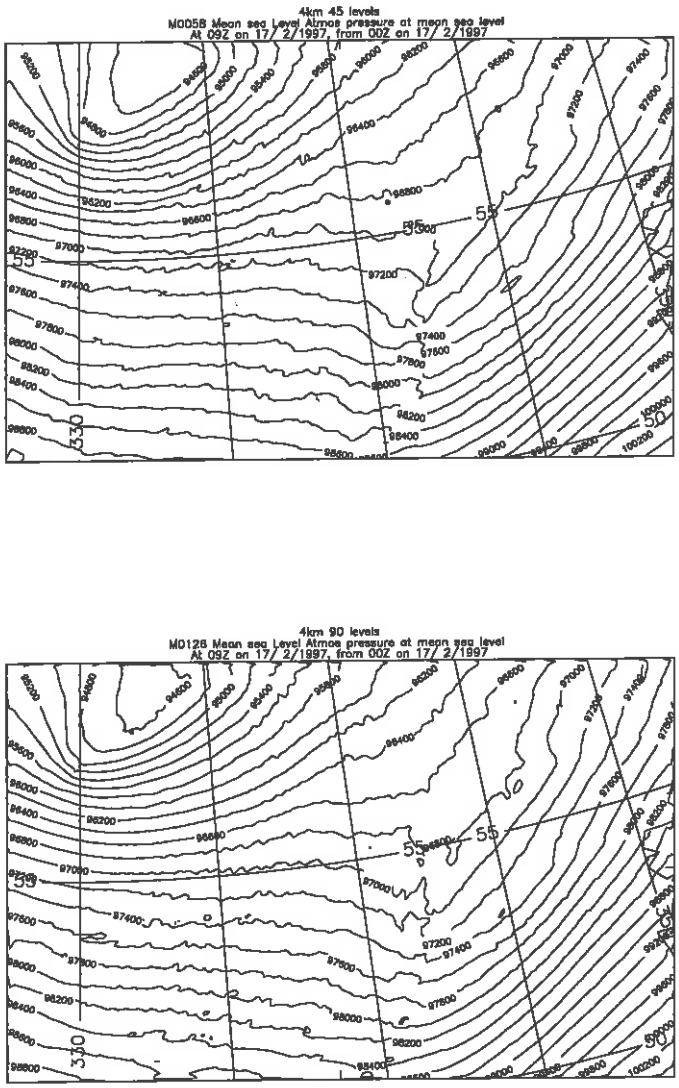

Figure 6.1 Comparison of pmsl in 4km 45 level and 90 level models

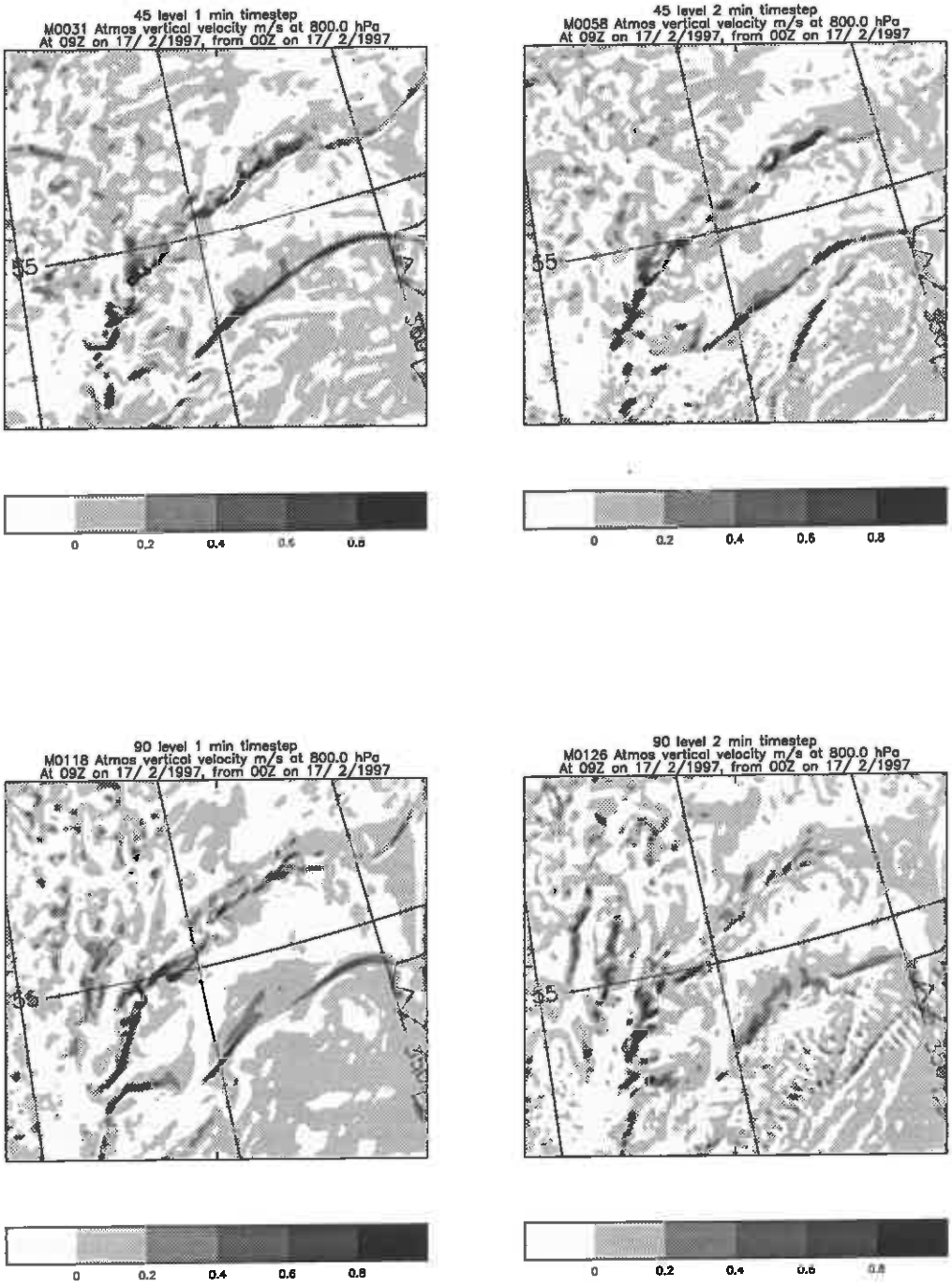

Figure 6.2 Comparison of 800mb vertical velocity fields in 4km models with 45 and 90 levels and 1 and 2 minute timesteps.

The 90 level model is clearly broadly similar to the 45 level one. Since the system is rapidly developing and develops from being just a trough in the model run this is implies that the two models are very similar. A more sensitive guide to the model performance is the 800mb vertical velocity fields which clearly show the double frontal structure of the system. A comparison of the two models is shown in figure 6.2. The figure also includes comparison of 1 and 2 minute timesteps since this has a bearing on the comparison. For a 1 minute timestep the 90 level and 45 level models are again broadly similar but the northern front becomes much more continuous at the rear of the system. It is not clear if this is a good thing from the observations – the breaking up of the front might well be what is expected in the real system. Furthermore in other parts of the system (e.g. the southern front and the forward part of the northern one) there are more breaks in the front in the 90 level run. The figure also shows that for the 2 minute timestep the model appears to be significantly degraded by going to 90 levels. It would be expected that the slantwise circulations seen in this system might be more sensitive to the increase in vertical resolution. This is shown in figure 6.3

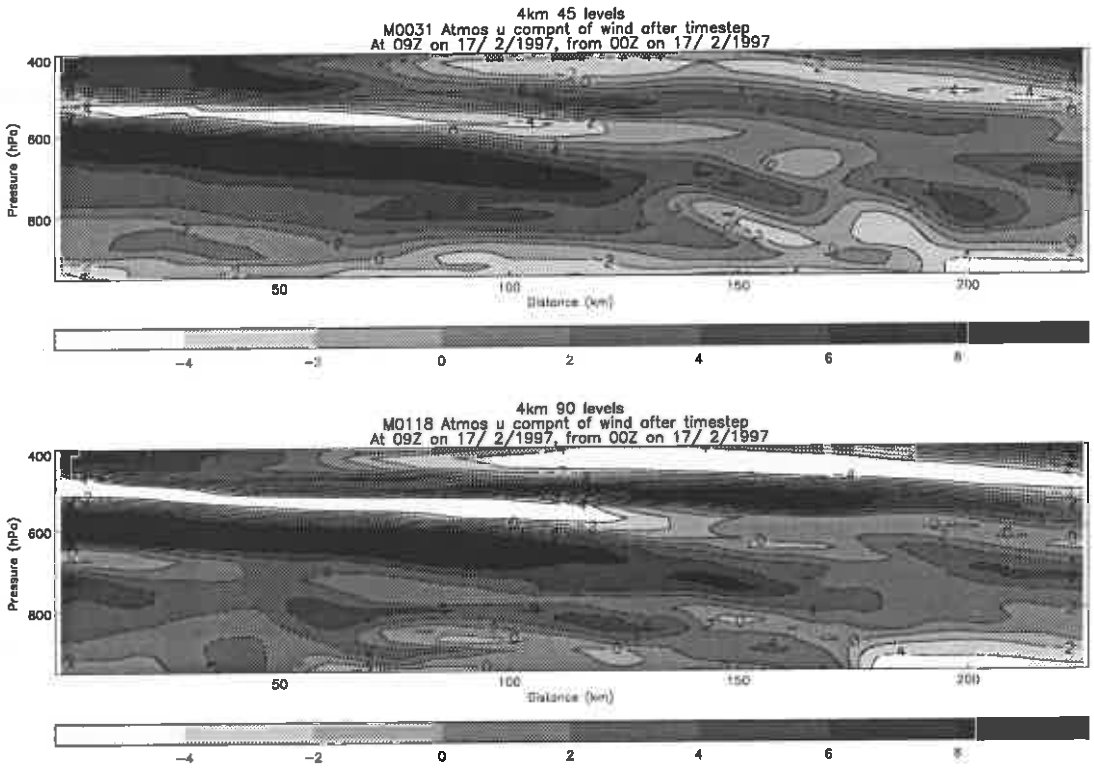

Figure 6.3 Cross section of cross frontal velocity along section which crosses the northern front. Light colours indicate motion towards left of figure.

The figure shows a cross section which crosses the northern front and in both cases a strong slantwise ascent and corresponding descent below can be seen associated with this front. (It is also possible to see the circulation from the southern front at the top right hand side of the section). The circulations become somewhat narrower (in the vertical) and more intense in the 90 level model as would be expected. In addition

there is a hint of a secondary circulations visible as additional layering below the primary one from the front. However, in contrast to what is seen with 2km horizontal gridlength (described in the next section) the overall difference between the 45 and 90 level is not great.

6.2 2km Model

We now consider the effect of vertical resolution in the 2km model. In this case we do not show the two pmsl fields since the 2km domain is quite small compared to the system and, as in the 4km model, the fields are very similar anyway. Figure 3.4 shows a comparison of the 800hPa vertical velocity fields. When looking at these charts it should be remembered that the scale is very cut down to show the detail – the magnitude of the vertical velocity along the line convection at the front is about 5m/s at its peak. The spin up of convection at the western boundary is a very obvious feature in these charts – it is a result of this model running without a convection scheme whereas the model providing the boundary conditions was run with (and at lower resolution). The explicit convection therefore spins up after the air enters at the western boundary. The main difference which is apparent between the 45 and 90 level models is that the northern front is more continuous and less fragmented in the along front direction. Although it is not apparent with the scales chosen in this figure it is also true that there is more banding in the across front direction in the 90 level model. This can be seen somewhat more clearly in the top right hand corner of figure 6.5 which shows the large scale precipitation rate in the two models.

This banding is consistent with the cross frontal velocity cross section along the line shown in figure 6.4 which is shown in figure 6.6. The cross section shows clearly that in the 90 level model the slantwise ascent at the front is better defined, more steeply sloping and breaking up into a number of separate circulations. On the right hand side of the cross sections it is also evident that the flow from the southern front (not included in the cross sections) has also split into two separate circulations. The cross section has deliberately been taken where the splitting of these flows is most evident. It is not surprising that this is right at top right hand corner of the domain since this is the area where the air surrounding the front has been in the domain of the high resolution model for the longest. Further back in the system similar features can be seen but less well defined (this is shown in section 4.2 where the comparisons of these features with observations are discussed). The 90 level model cross section was obtained from a model running with a 15s timestep. A timestep this short was found to be necessary to obtain the observed coherent slantwise features although runs with longer timesteps still had the same degree of layering.

Figure 6.6 also includes an equivalent cross section taken from the 135 level model. This model was run in order to ascertain whether the layers/circulations would split even further if the vertical resolution was increased. It can be seen that the factor of 1.5 increase in resolution changes some of the details of the slantwise structures but their number and number of vertical layers remains unchanged. There is therefore an encouraging implication of convergence with regard to the vertical resolution. In order to get coherent slantwise structures it was found necessary to run with a 10s timestep in the 135 level model.

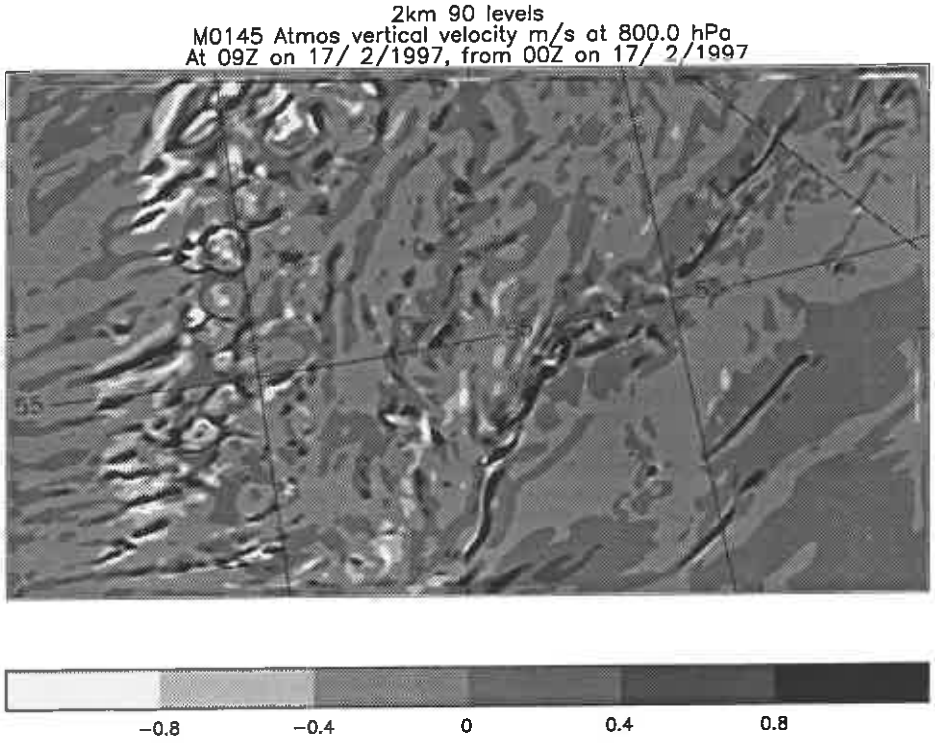

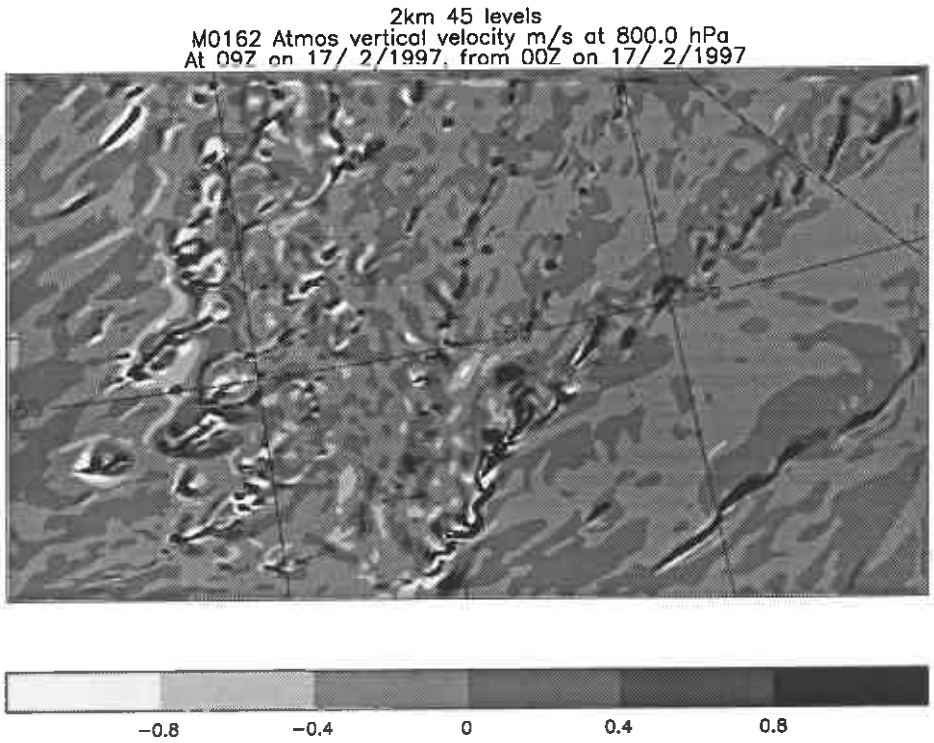

Figure 6.4. Comparison of 90 level and 45 level 2km runs.

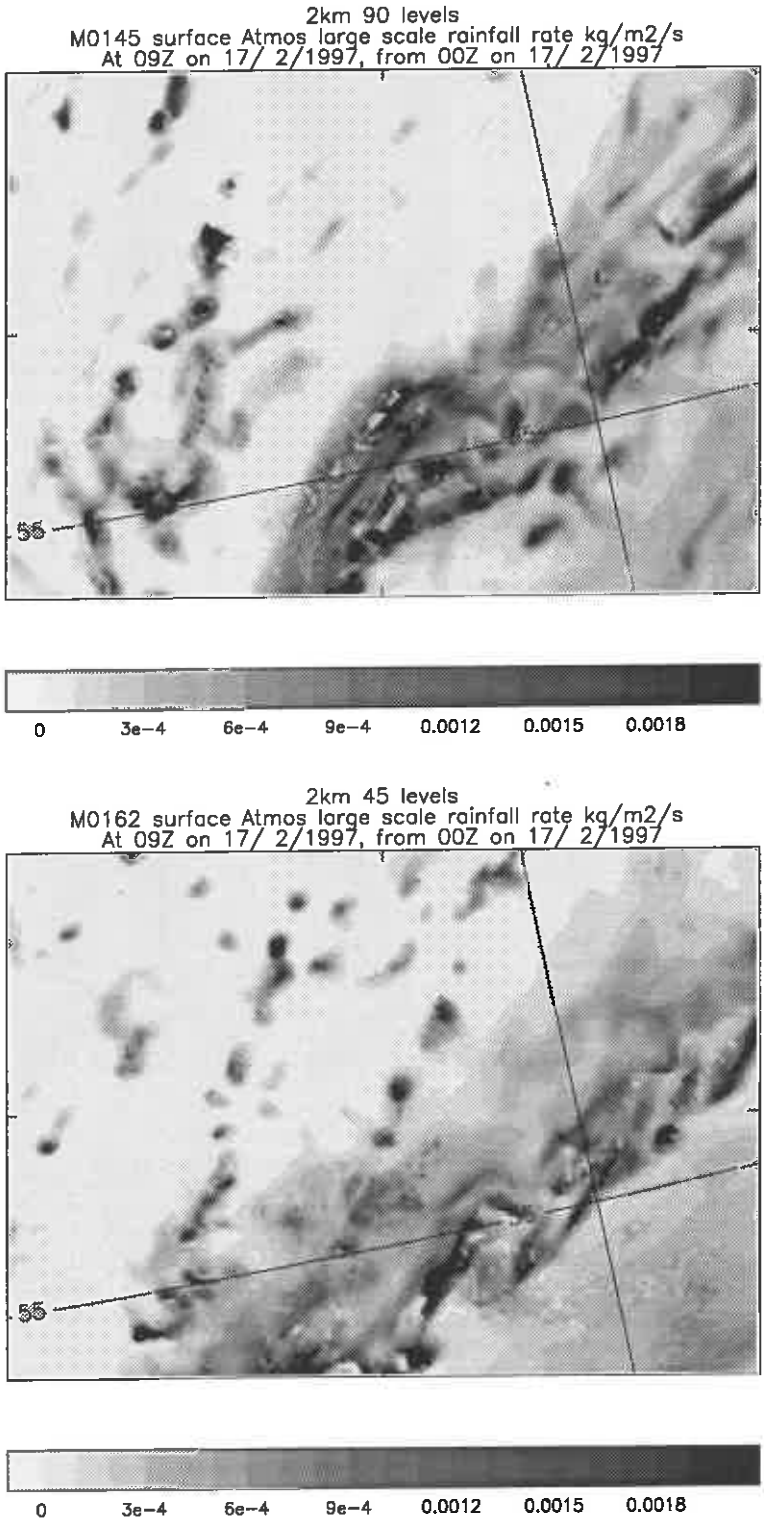

Figure 6.5 Large Scale rainrate in part of domain for 2km 90 and 45 level models.

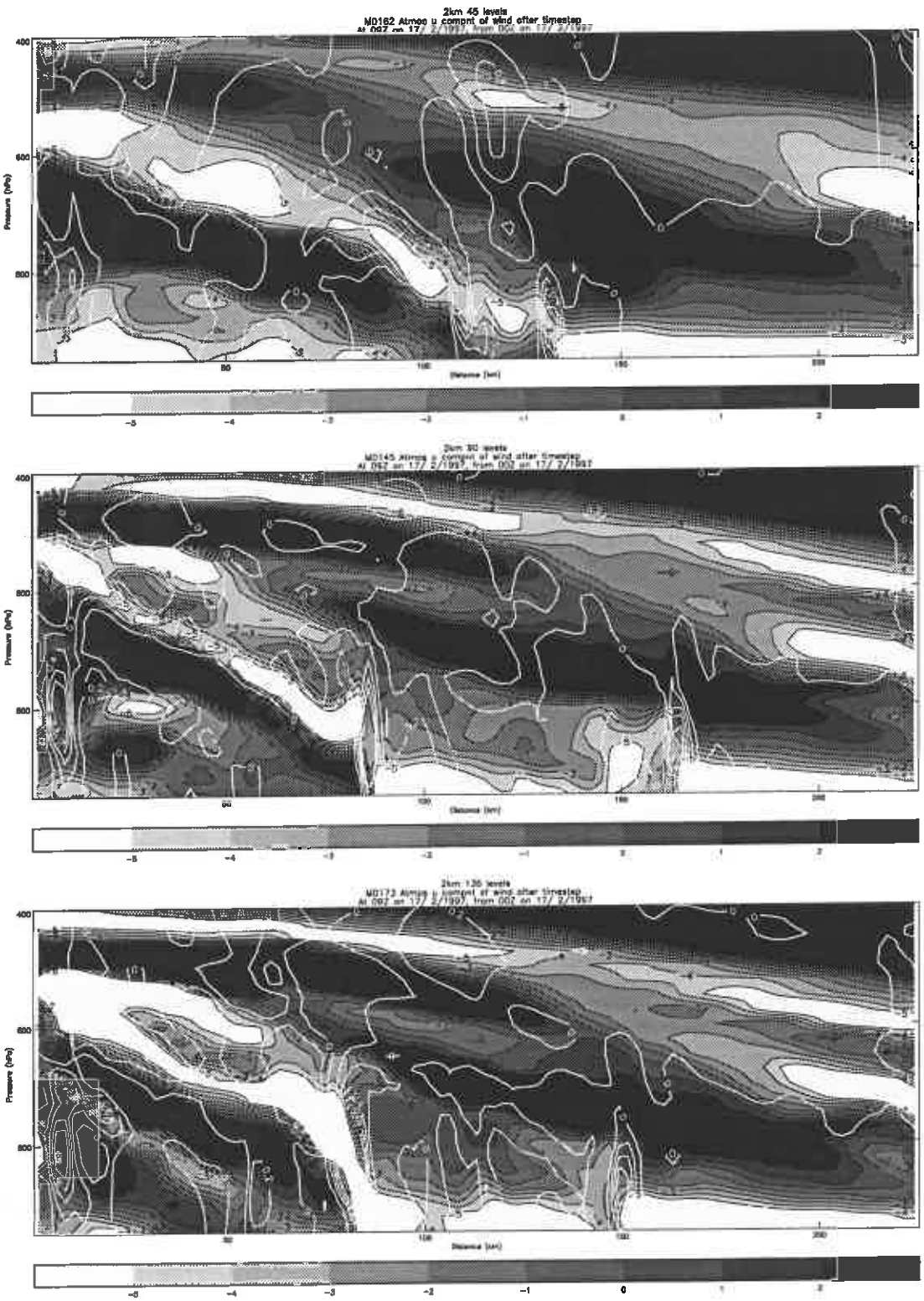

Figure 6.6 Cross sections along line in fig 3.4 of cross frontal velocity (shading, white=towards left) and vertical velocity (white contours) for 2km 45,90 and 135 level models.

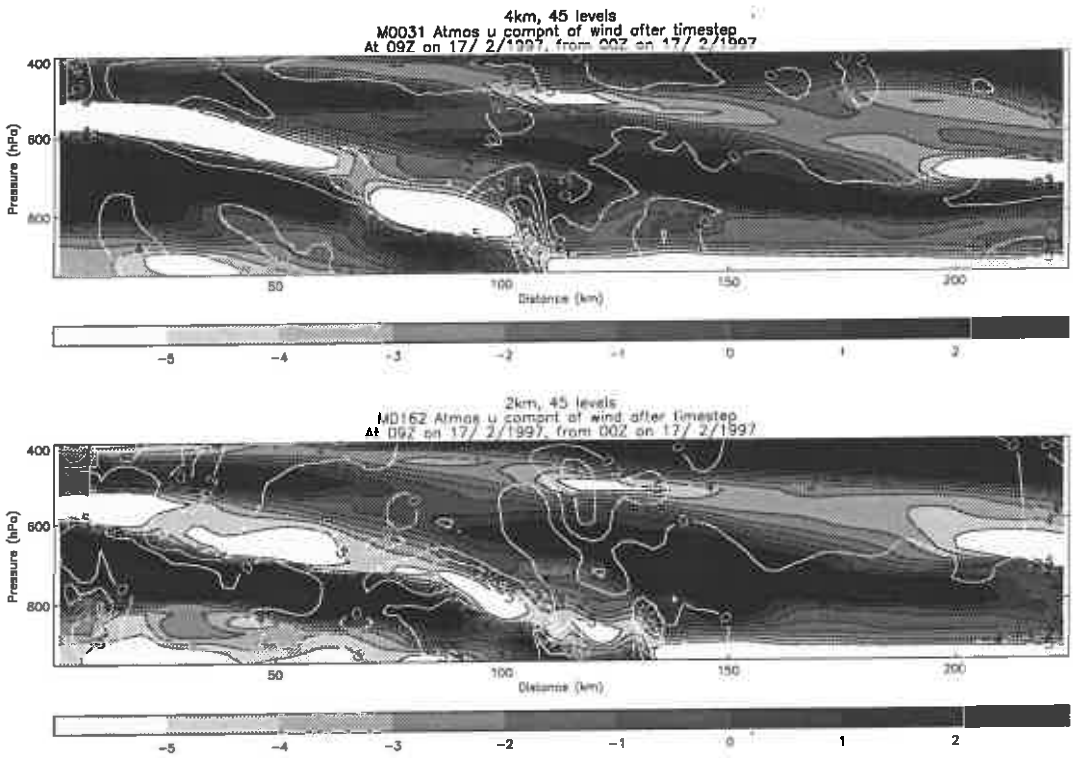

Figure 6.7 Cross sections along line in fig3.4 of cross frontal velocity (shading, white towards left) and vertical velocity (white contours) for 4 and 2km 45 level models (for comparison with fig6.8)

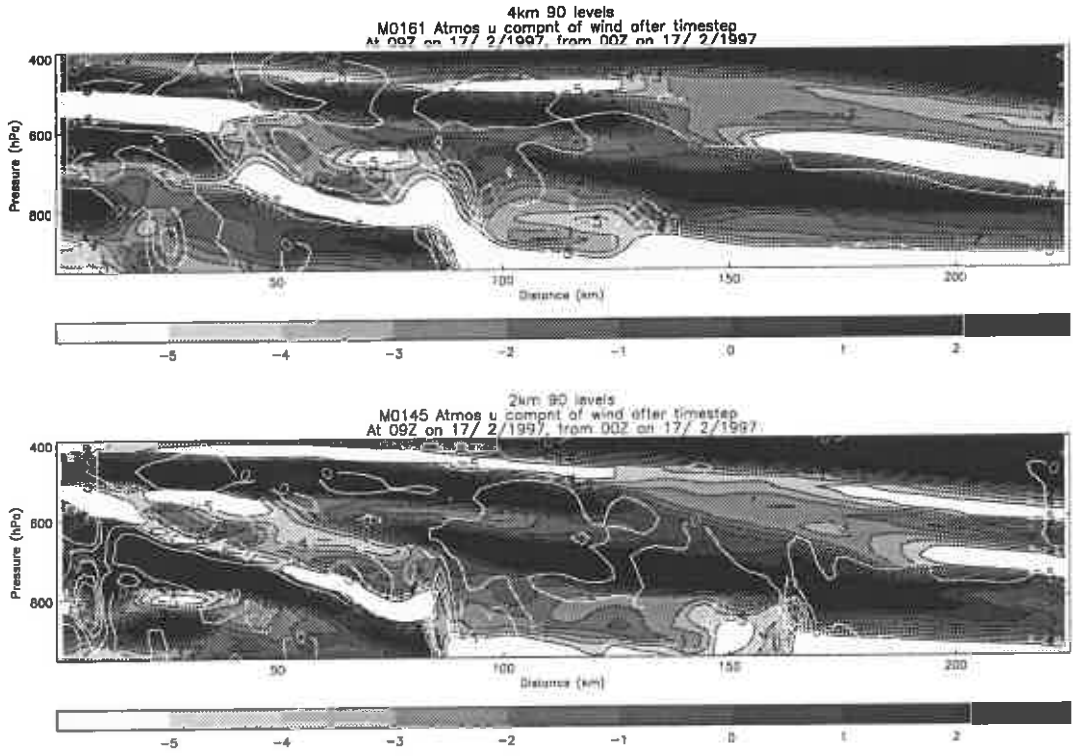

Figure 6.8 As figure 3.7 but for 90 level models.

6.3 General Comparisons

It is noticeable from the above that there is a much more dramatic change (certainly as regards the slantwise circulations) going from 45 to 90 levels at 2km horizontal gridlength than at 4km. A related observation is that going from 4km to 2km only produces significant benefit in this particular case if 90 levels are used rather than 45. This is illustrated by figures 6.7 and 6.8 which shows a comparison of the same cross section in 4 and 2km models with 45 and 90 levels respectively. In the 45 level models a single slantwise ascent can be seen from the northern front with no sign of the splitting seen with 90 levels. It would appear that it is worthwhile going to 90 levels for a 2km model but probably not for a 4km one, at least as far as features seen in this case are concerned. As seen in the last section increasing the number of levels at 4km gridlength may even be detrimental if a long timestep is being used.

6.4 Discussion of 2km results

It is reasonable to ask if the observed dramatic difference in the representation of the slantwise features in the 2km model between the 45 and 90 level model is understandable. This question is addressed in this section.

The first consideration is simply to compare the vertical spacing of the layers which appear when the circulations split to spacing of the levels in the model. In figure 6.6 the vertical separation between adjacent maxima of the upwards slantwise flows is approximately 100hPa (about 1100m) which corresponds to around 3-4 levels in the 45 level model. Clearly between the two upwards maxima the model has to represent the intervening downwards maxima so the 45 level model would have difficulty resolving these phenomena. In contrast the 90 level model would have 7-8 levels in the same vertical space which would appear much more likely to resolve the structures.

A second consideration is the horizontal/vertical grid aspect ratio as compared to the slope of the features under consideration. Persson and Warner (1991) define a dimensionless quantity AS which is the ratio of the grid aspect ratio to the slope of the feature of interest ie $AS \equiv (\Delta p/\Delta s)/s$ where Δp is the vertical grid spacing, Δs is the horizontal and s is the slope of the feature of interest. In this case the slope of the slantwise ascents is approximately 3.1 hPa/km which give values of the AS for the 2km models shown in table 6.1. Intuitively one would expect the best representation for the case AS=1 in which case the grid is matched to the slope of the feature. This is borne out by the analysis of Persson and Warner who conclude that the vertical resolution of the model should ideally be sufficient to give AS=1. For AS>1 the mismatch between the grid and the sloping feature will generate spurious gravity waves although these will be very small and may normally be ignored if AS <2.

MODEL	Res (700hPa)/Pa	Grid Aspect Ratio HPa/km	AS
45 level	28.2	14.1	4.5
90 level	14.1	7.3	2.3
135 level	8.6	4.3	1.4

Table 6.1. Grid aspect ratios for the 2km models for slantwise ascent with a gradient of 3.1hPa/Km. AS is as defined in text.

Although we have not carried out detailed analysis of this aspect it is noticeable that according to this analysis we would expect the 90 and 135 level models to be suffer significantly less from spurious gravity waves than the 45 level one. One could speculate that the extra breaking up of the fronts observed in the 45 level model (figure 6.4) could be in part due to the extra gravity wave generation by the mismatch of the grid aspect ratio to the slope of the slantwise ascent.

7. Comparisons to Observations

This section presents comparisons of the model to observations. Since the most dramatic changes to the model with vertical resolution were seen with the 2km model the comparisons are limited to this model.

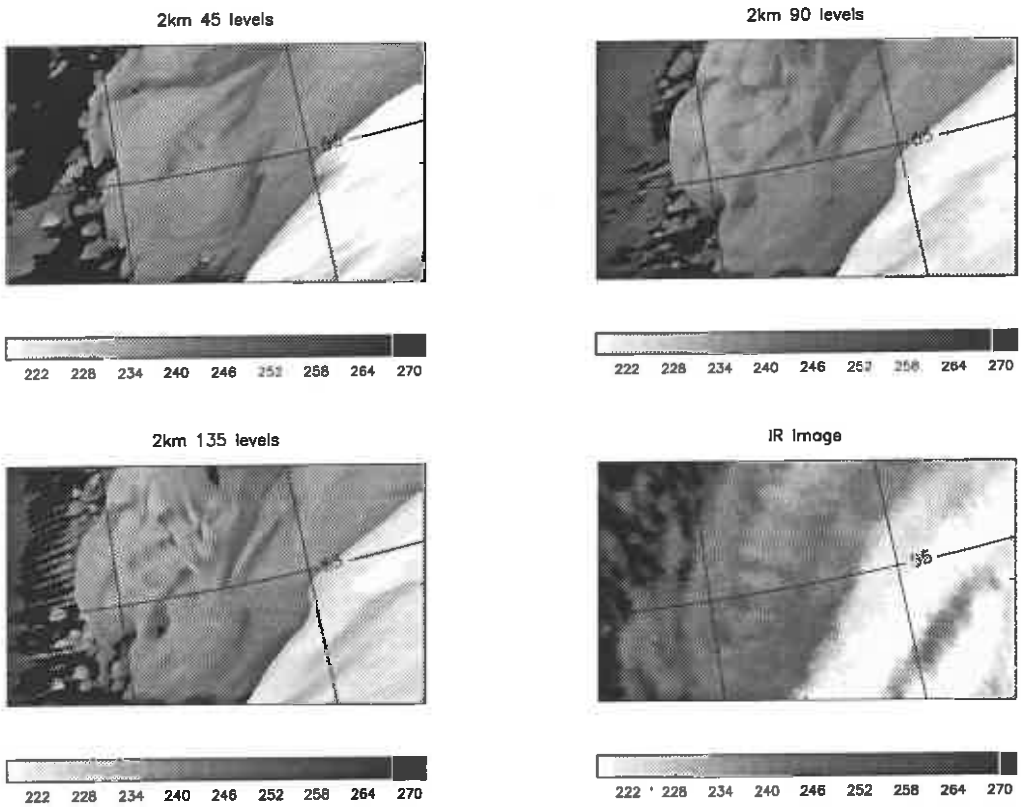

Figure 7.1 Cloud top temperatures for 2km 45, 90 and 135 level models and IR image.

7.1 Satellite Imagery

Figure 7.1 Shows a comparison between the cloud top temperatures in the 45 and 90 level 2km models with the corresponding IR image. The figure is included because it is the easiest comparison with observations. However it again implies that there is little to choose between the models. Unsurprisingly the errors in the models make the model simulations much more like each other than like the IR image. The model cloud heads are all overdeveloped compared to the imagery (the obvious cloud heads

in the model actually correspond to the small secondary one on the extreme left of the satellite image). Despite this it is still noticeable that increasing the vertical resolution increases the variability of the cloud which makes it appear more like the observations.

7.2 FASTEX Dropsondes

The UK C-130 aircraft dropped sondes into the system in a systematic scan of the system between 6 and 12Z consisting of six runs in the across front direction. An objective analysis technique has been used with this dropsonde data in order to produce cross sections (Forbes et al 2000ii). These cross sections are, however, not discussed here since due to the spacing of the sondes the full structures in the vertical are not apparent. In order to see full structures in the vertical it is necessary to look at data from individual sondes.

Figure 7.2 shows a hodograph from a sonde at 6:40Z in a position just to the north of the northern front. The hodograph shows the two main flows from the two fronts (marked A and B on the figure) and in addition the flow from the northern most front shows one or two secondary flows (depending on whether the flow at low levels counts as one). Similar structures were seen in a number of dropsondes which were similarly placed relative to the fronts. We now compare this data with that from the 90 level model which shows the splitting of the flow from the northern front in the cross sections (the 45 level model is not compared in this way since we know from the cross sections that the flow is not split).

Figure 7.3 shows a model hodograph which is the best estimate for the model at the same time (correcting for the system position). The model hodograph shows similar features to the dropsonde one (i.e. an upper flow and several ones at lower levels) only more weakly and not at the correct levels. The weakness of the features is explained by the fact that in order to find the position most likely to correspond to the dropsonde a position was chosen about half way along the model domain. As mentioned in section 6.2 the slantwise features became more evident as the air moves across the 2km model presumably corresponding to the time the model takes to spin them up. In order to emphasise this point figure 7.4 shows a hodograph taken from a point to the north of the northern front on the cross section position shown in fig 6.4. The cross frontal flows (in particular the splitting of the flows from the northern front) now show up much more clearly as would be expected from the cross sections.

We conclude that the splitting of the cross frontal slantwise flow from the northern front in the 90 level model appears very similar to that seen in the observations from several dropsondes. From the comparisons shown in section 6.2 we can safely assume that the very similar results obtained in the 135 level model would also be in agreement with observations.

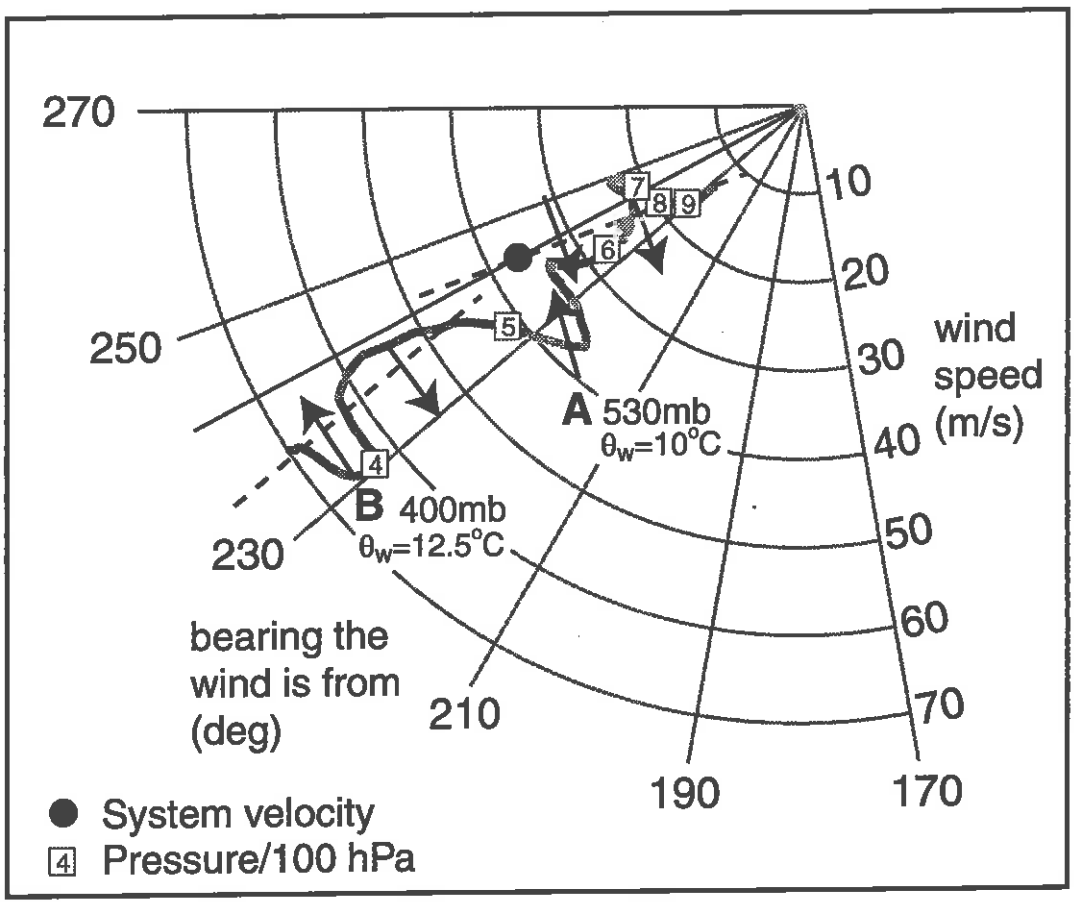

Figure 7.2 Dropsonde Hodograph showing multiple circulations.

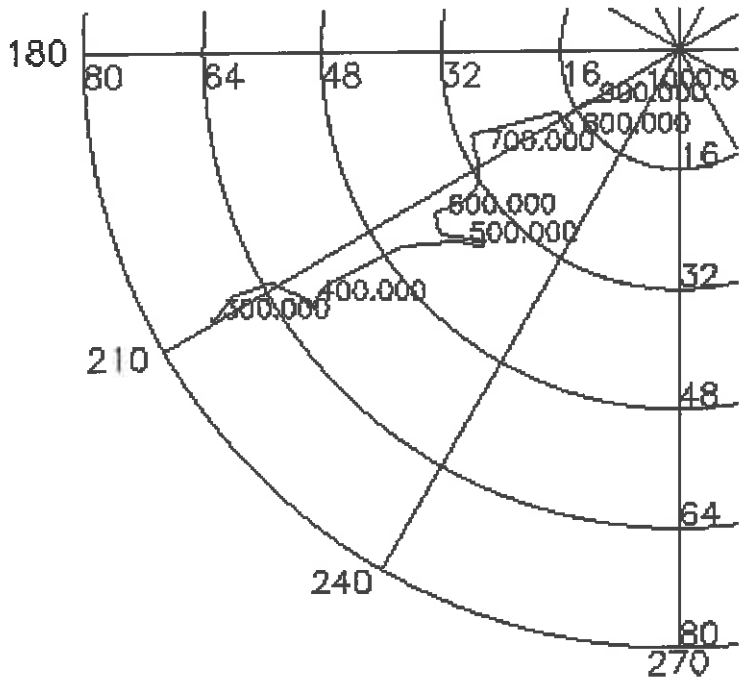

Figure 7.3 Model hodograph for 6:30Z at best estimate of position corresponding to that in figure 7.2

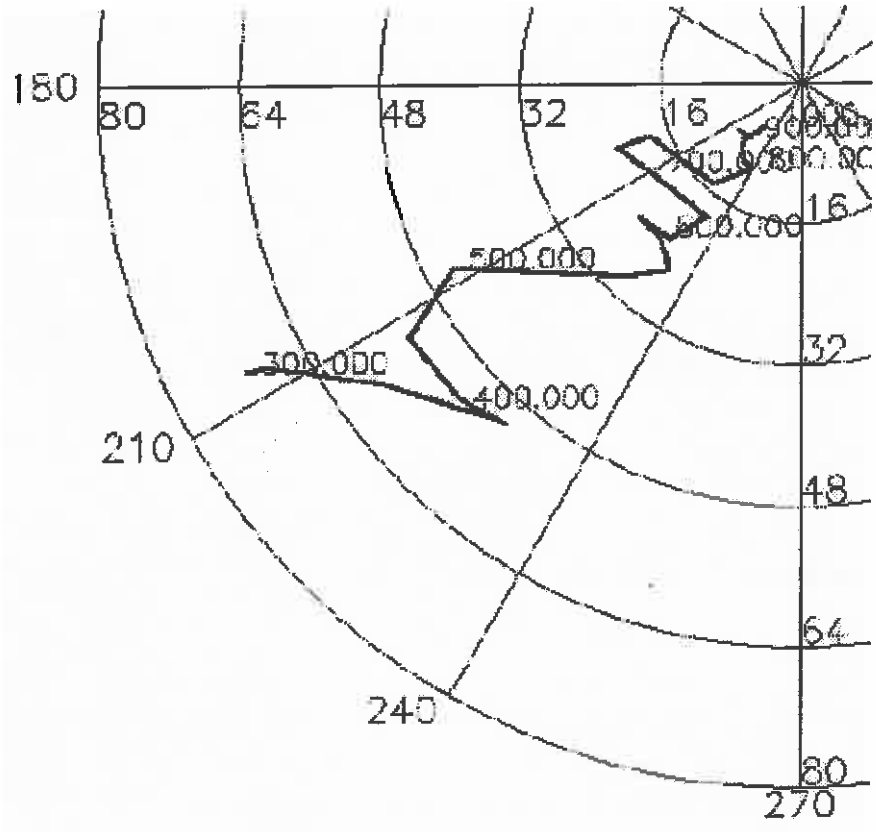

Figure 7.4 Model hodograph for 9Z at position on cross section in figure 6.4

8. Conclusions

The New Dynamics model has been run at various horizontal and vertical resolutions on the FASTEX IOP16. Two systematic studies have been carried out on varying horizontal and vertical resolution.

8.1 Horizontal Resolution

The model has been run with gridlengths of 60,24,12,4 and 2km. As the gridlength is reduced many more realistic features are produced by the model. Examples of this are that the fronts split in the across front direction and also into cells in the along front direction.

If the vertical velocity and pmsl fields from the various resolution models are area averaged to 60km gridlength the results look very similar to the eye. More quantitatively, the average upward vertical velocity on 60km scales is approximately constant as the gridlength is changed. This implies that, despite all the extra structure in the high resolution models these are still consistent with the subgrid parameterisations in the lower resolutions ones. In contrast if the average upward vertical velocity is calculated without first averaging to 60km scales there is a strong

upward trend as the resolution is increased which implies the model has some knowledge of subgridscale structure (ie it appears to take into account the varying amount of background subsidence in the different sized gridboxes). The upwards flux on part of the northern front was calculated and tends to a constant as the resolution is increased as long as the models convection scheme is suppressed. Energy spectra of the same vertical velocity fields show a turn up at the shortest wavelengths for all but the 2km and 60km runs which implies that the other models are suffering some aliasing of subgridscale structure onto the gridscale. (Comparison of spectra of a domain not including the fronts shows that this aliasing is taking place at the line convection on the fronts). If the power spectra are divided by the 2km one and renormalised according to the gridlength then it is found that there is a consistent filter function as scales reduce towards the gridlength. The implication is that the representation of any feature smaller than about 5 gridlengths is attenuated.

Comparisons were also made of the cloud ice, cloud liquid water and the various precipitation fields. The cloud ice increases significantly decreasing gridlength below 24km which corresponds to the larger average upward vertical velocities in the higher resolution models. The cloud water also changes significantly. More work needs to be carried out on both the cloud ice and cloud water from this point of view. Comparisons of the precipitation rates show that, as expected the convective component decreases and the large scale component increases as the gridlength is reduced. The sum of the two, however, stays relatively constant and, at 4 and 2km, is close to the value of the large scale precipitation rate in runs with the convection scheme suppressed by having a long cape closure timescale.

8.2 Vertical Resolution

A comparison has been made between models with 45, 90 and 135 vertical levels. In general it is observed that there is not much change in the model in increasing the vertical resolution (particularly at 4km gridlength). However at 2km gridlength it is found that the cross frontal slantwise circulations split into a number of separate circulations when going from 45 to 90 levels. Increasing the vertical resolution further to 135 levels does not produce a further significant change. The splitting of the slantwise structures is in agreement with data from dropsondes.

A corollary to this is that it is not worth decreasing the horizontal gridlength from 4km to 2km without increasing the vertical resolution from 45 levels. This conclusion, however, is likely to be specific to the representation of slantwise structures on these scales – the slantwise circulations were the feature which changed most with vertical resolution. For other purposes 45 levels may well be adequate.

References

R Forbes, H Lean, N Roberts and P Clark (2000) JCMM Internal Report 107 "Implications for Mesoscale Modelling from a Study of the FASTEX IOP16 Mid-latitude Cyclone"

H Lean (2000) JCMM Internal Report 119/NWP Forecasting Research Technical Report no 320 "Tests of New Dynamics Model on the FASTEX IOP16 Case"

P.Persson and T Warner Mon. Wea. Rev. **119** (1991) 917-935 "Model Generation of Spurious Gravity Waves due to Inconsistency of the Vertical and Horizontal Resolution"

ANNEX A

Deductions from the Curves of Average Upward Vertical Velocity

In this annex we investigate what would be expected to be seen in models of varying resolution when attempting to represent an assumed distribution of vertical velocity in the atmosphere.

We start with the assumption that the atmosphere that the models are trying to represent consists of (in 1 dimension) an array of delta functions with uniform subsidence in-between such that the total upward velocity flux is zero. We assume that the delta functions are randomly distributed but with an average spacing λ which is assumed to be greater than the model gridlength, dx. Assume the upwards flux due to the delta function vertical velocity is I so that the subsidence between the delta functions is I/λ.The relevance of these assumptions to the real situation is discussed later.

Firstly we consider what we would expect to see if we carry out the procedure used to obtain the graph shown in figure 3.6. This was to average the values at all the gridpoints having set any with negative values to zero. The central issue is how the model with a gridlength dx would be expected to represent a "real" distribution which is a delta function of upwards motion with subsidence elsewhere. There are two extreme cases. In the best case the model would correctly average over the distribution within the gridbox ie the total upward flux in the gridbox would consist of the upward flux from delta function minus a contribution from the subsidence between. This clearly implies that the model has a knowledge of the subgridscale structure either from the large scale or from parameterisations. A second possible response of the model would be to alias the upwards vertical velocity onto the whole gridpoint – ie the gridpoint will have upwards velocity with the total upwards flux over the gridpoint equal to that from the delta function. In this case the effect of the subsidence within the gridbox would be lost and it is this which leads to the difference between the two types of model on averaging up. In both cases only gridpoints containing the delta function upward vertical velocity spikes need be considered since the others will have negative overall vertical velocity and hence be set to zero before averaging. The gridpoints containing the upward vertical velocity spikes will have an increasing upward flux as the gridlength is reduced in the model which takes into account subgrid fluxes because the smaller the gridbox the less of the negative flux between delta functions is included. The upwards vertical flux in the gridbox is therefore $I(1-dx/\lambda)$. In order to obtain the average vertical velocity we multiply this by dx/λ, the fraction of boxes which contain the upwards vertical velocity spikes, and divide by dx to convert from flux to vertical velocity and obtain $w_{av}=(I/\lambda)(1-dx/\lambda)$ which increases as dx decreases. Conversely in the case where the upwards vertical velocity is simply aliased onto the whole gridpoint the upward flux will be unchanged with resolution since the upwards vertical flux in the gridboxes containing the spikes will then be I regardless of resolution leading to the corresponding expression for the

average $w_{av}=(I/\lambda)$ which is unchanged with resolution. If $dx>\lambda$ it is clear that for the model which correctly deals with the subgrid structure the average will continue to decrease as the gridlength increases due to increased cancellation between the positive spikes and the negative background. It is not so clear in this case what a model which tends to alias vertical velocity would do. However the upward trend in the curve in fig 3.6 is consistent with the conclusion that the model does, to some degree, take into account subgrid effects.

A similar conclusion can also be obtained if we consider the averaging of the type shown in figure 3.5 where the vertical velocity data was averaged onto a coarser grid, spacing DX (60km), before setting any negative values to zero and then averaging. In this case it is clear that the model which takes into account subgrid structure will give the same average whatever the resolution since the total flux in the large gridbox, DX, will be unchanged whatever the size of the model gridboxes. In the case where the model aliases the upward vertical velocity spike onto the gridbox scale the average actually decreases as the model gridboxes shrink since the DX sized gridbox includes a slightly larger area of subsidence. This is true if DX is greater or smaller than λ. The curve in figure 3.5, then, also provides evidence that the model doesn't simply alias vertical velocity onto the gridlength since it gently increases and tends to become constant as the gridlength is reduced rather than falling.

It is important to consider how relevant this model is to the case under consideration and whether there are any other effects which could dominate over the one considered to influence the shapes of the curves. The model of delta function areas of updraft and uniform subsidence may not appear to be that relevant to the real situation. In practice a look at the fields from the high resolution models shows that there are some regions of concentrated downdraft as well as those of concentrated updraft. There are regions of downdraft associated with the line convection at the fronts and downdrafts associated with the convection behind the system (which are more obvious given that we are considering the vertical velocity at a relatively low level). If we modify our model of the real situation to include negative delta functions as well as positive the main effect this has on the argument is the resulting reduction in the uniform subsidence which has been assumed (since the negative delta functions themselves will be set to zero before averaging). In the most extreme case where the negative delta functions contain the same downward flux as the upward ones the background value would become zero. This would mean that the differences between the subgrid model and the aliasing one would disappear since they depended on including different amounts of the negative subsidence.

We have attempted to test the validity of this simple model by looking at the 2km data and calculating the effect of averaging it up to 4km. If we take the 2km model over the area used for the averaging in fig 3.6 we can get an idea of the magnitude of the background (ie the value of vertical velocity NOT in the positive or negative peaks) by averaging all the values which are above $-0.2ms^{-1}$ but below $0.2ms^{-1}$. This gives an average value of $-0.0021ms^{-1}$. Similarly we can calculate the average value for the vertical velocity in the positive peaks by averaging over all values greater than $0.2ms^{-1}$ – this gives a value of 0.65ms. We can form an area average equivalent to that in fig 3.6 by considering the points with values above $0.2ms^{-1}$ and assuming that all other points have value zero. This ignores any non-zero points in the background values (between $0.2ms^{-1}$ and zero) and the effect that this has is discussed later. The

result of this is that the average upward vertical velocity for the 2km model is $0.078ms^{-1}$ We now consider a 4km model which we assume correctly takes account of the subgrid structure. In order to calculate the value for this we therefore need to assume that each 2km gridpoint with vertical velocity above $0.2ms^{-1}$ is grouped with three with the average (negative) background value. This assumes the delta function model – ie the points with values above $0.2ms^{-1}$ are not grouped together which is certainly not the case – One might hope, however, that where there are coherent structures such as fronts the whole feature might broaden in the lower resolution model thus including more of the background and, to some degree, reducing this error. When the average is so calculated for the assumed 4km model the result is $0.072ms^{-1}$ ie $0.006ms^{-1}$ below the value from the 2km model. This shows reasonable agreement with fig3.6 where the average increases by about $0.01ms^{-1}$ between the 4km and 2km models. We now address the problem mentioned earlier that this argument has neglected the contribution to the average from the background values between zero and $0.2ms^{-1}$ (the points below zero are irrelevant since they are set to zero). In the 2km model the points in this range average to a value of $0.074ms^{-1}$ and in the 4km one (the real 4km model as opposed to the assumed one) they average to $0.071ms^{-1}$. Only about a third of the model gridpoints have these values so when averaged over the whole area these represent contributions to the overall average of 0.0246 and $0.0230ms^{-1}$ respectively. The difference between these is only of order 0.001 which is a tenth of the difference observed.

In conclusion, the arguments presented in this appendix have shown that the curves shown in figs 3.5 and 3.6 appear to be consistent with the models correctly accounting for subgridscale effects. This assumes a simplistic model of the atmosphere consisting of delta function regions of ascent with uniform subsidence in-between. Analysis of data from the 2km model and comparison to the 4km model implies that this may not be an unreasonable assumption.

CURRENT JCMM INTERNAL REPORTS

This series of JCMM Internal Reports, initiated in 1993, contains unpublished reports and also versions of articles submitted for publication. The complete set of Internal Reports is available from the National Meteorological Library on loan, if required.

1. **Research strategy and programme**
   K A Browning et al
   January 1993

2. **The GEWEX Cloud System Study (GCSS)**
   GEWEX Cloud System Science Team
   January 1993

3. **Evolution of a mesoscale upper tropospheric vorticity maximum and comma cloud from a cloud-free two dimensional potential vorticity anomaly**
   K A Browning
   January 1993

4. **The global energy and water cycle**
   K A Browning
   July 1993

5. **Structure of a midlatitude cyclone before occlusion**
   K A Browning and N Roberts
   July 1993

6. **Developments in systems and tools for weather forecasting**
   K A Browning and G Szejwach
   July 1993

7. **Diagnostic study of a narrow cold frontal rainband and severe winds associated with a stratospheric intrusion**
   K A Browning and R Reynolds
   August 1993

8. **Survey of perceived priority issues in the parametrizations of cloud-related processes in GCMs**
   K A Browning
   September 1993

9. **The effect of rain on longwave radiation**
   I Dharssi
   September 1993

10. **Cloud microphysical processes - a description of the parametrization used in the large eddy model**
    H Swann
    October 1993

11. **An appreciation of the meteorological research of Ernst Kleinschmidt**
    A J Thorpe
    May 1992

12. **Potential vorticity of flow along the Alps**
    A J Thorpe, H Volkert and Dietrich Heimann
    August 1992

13. **The representation of fronts**
    A J Thorpe
    January 1993

14. **A parametrization scheme for symmetric instability: test for an idealised flow**
C S Chan and A J Thorpe
February 1993

15. **The Fronts 92 Experiment: a Quicklook Atlas**
Edited by T D Hewson
November 1993

16. **Frontal wave stability during moist deformation frontogenesis**
Part 1: Linear wave dynamics
C H Bishop and A J Thorpe
May 1993

17. **Frontal wave stability during moist deformation frontogenesis**
Part 2. The suppression of non-linear wave development
C H Bishop and A J Thorpe
May 1993

18. **Gravity waves in sheared ducts**
S Monserrat and A J Thorpe
October 1993

19. **Potential vorticity and the electrostatics analogy: quasi-geostrophic theory**
C Bishop and A J Thorpe
November 1993

20. **Recent advances in the measurement of precipitation by radar**
A J Illingworth
April 1993

21. **Micro-physique et givrage: cloud microphysics and aircraft icing**
A J Illingworth
May 1993

22. **Differential phase measurements of precipitation**
M Blackman and A J Illingworth
May 1993

23. **Estimation of effective radius of cloud particles from the radar reflectivity**
N I Fox and A J Illingworth
May 1993

24. **A simple method of Dopplerising a pulsed magnetron radar**
A Hua, A J Illingworth and J Eastment
November 1993

25. **Radiation and polar lows**
George C Craig
February 1994

26. **Collected preprints submitted to the International Symposium on the Life Cycles of Extratropical Cyclones; Bergen, Norway, 27 June - 1 July 1994**
April 1994

27. **Convective frontogenesis**
Douglas J Parker and Alan J Thorpe
April 1994

28. **Improved measurement of the ice water content in cirrus using a total water evaporator**
Philip R A Brown and Peter N Francis
April 1994

29. **Mesoscale effects of a dry intrusion within a vigorous cyclone**
K A Browning and B W Golding
April 1994

30. **GEWEX Cloud System Study, Science Plan**
May 1994

31. **Parametrization of momentum transport by convectively generated gravity waves**
R Kershaw
May 1994

32. **Mesoscale Modelling Newsletter No 5**
May 1994

33. **Observations of the mesoscale sub-structure in the cold air of a developing frontal cyclone**
K A Browning, S A Clough, C S A Davitt, N M Roberts and T D Hewson
May 1994

34. **Longwave radiative forcing of a simulated tropical squall line**
Imtiaz Dharssi
July 1994

35. **On the nature of the convective circulation at a kata-cold front**
K A Browning
September 1994

36. **Collective preprints of papers submitted to the COST-75 International Seminar on Advanced Weather Radar Systems, Brussels, 20-23 September 1994**
November 1994

37. **Use of satellite imagery to diagnose events leading to frontal thunderstorms: Parts I and II of a case study**
K A Browning and N M Roberts
November 1994

38. **The role of spaceborne millimetre-wave radar in the global monitoring of ice cloud**
P R A Brown, A J Illingworth, A J Heymsfield, G M McFarquhar, K A Browning and M Gosset
December 1994

39. **Potential vorticity inversion**
Michal Ziemianski
October 1994

40. **Theory of mature tropical cyclones; a comparison between Kleinschmidt (1951) and Emanuel (1986)**
Suzanne L Gray
December 1994

41. **Dispersion and removal of pollutants during the passage of an atmospheric frontal system**
N R Gimson
December 1994

42. **The role of snow sublimation in frontogenesis**
D J Parker and A J Thorpe
December 1994

43. **Potential vorticity and the electrostatics Analogy: Ertel-Rossby formulation**
A J Thorpe and C H Bishop
December 1994

44. **Mesoscale aspect of extratropical cyclones: an observational perspective**
K A Browning
January 1995

45. **A polar low outbreak: evolution and mesoscale structures**
T D Hewson, G C Craig and C Claud
February 1995

46. **Generation of near-surface gusts of deep convection**
K Nakamura and R Kershaw
April 1995

47. **Attribution concepts applied to the Omega Equation**
S A Clough, C S A Davitt and A J Thorpe
June 1995

48. **Parametrization of mixed-phase cloud and precipitation**
Susan P Ballard and M Gerard Hutchinson
June 1995

49. **Short-range forecasting of stratocumulus: initialization prediction**
Susan P Ballard, Simon D Jackson and B Macpherson
June 1995

50. **Contributions of the JCMM/Dept of Meteorology Radar Group to the 27th AMS Radar Meteorology Conference, Vail October 1995**
June 1995

51. **Cold pools in shear**
Douglas J Parker
September 1995

52. **High-resolution analysis of frontal fracture**
K A Browning, S P Ballard and C S A Davitt
September 1995

53. **The albedo of broken cloud fields: calculations using a modified two stream radiation code**
Imtiaz Dharssi and Roy Kershaw
October 1995

54. **Parametrization of momentum transport by convection. I: theory and cloud modelling results**
R Kershaw and D Gregory
November 1995

55. **Variation of frontal structure along a cold front**
K A Browning and N M Roberts
November 1995

56. **Secondary frontal waves**
Douglas Parker
December 1995

57. **Objective fronts**
T D Hewson
March 1996

58. **Mesoscale analysis of the activation of a cold front during cyclogenesis**
K A Browning, N M Roberts and A J Illingworth
June 1996

59. **Investigation of different representations of rain in a 1-d evaporation model**
H Swann
May 1996

60. **Parametrization of diabatic processes in the inversion of the omega-equation**
M Athanassiadou and A J Thorpe
June 1996

61. **The role of the environmental flow in the development of secondary frontal cyclones**
I A Renfrew, A J Thorpe and A Joly
June 1996

62. **Consequences of the geostrophic momentum approximation on barotropic instability**
S Malardel, A J Thorpe and A Joly
June 1996

63. **Contributions to the AMS/RMS Conference on Mesoscale Processes**
Reading, 9-13 September 1996

64. **Vorticity and potential vorticity in stratified flows interacting with an isolated obstacle**
Jorge A Gutiérrez and A J Thorpe
September 1996

65. **Triple point development: two case studies**
Douglas Parker
September 1996

66. **Radar observations of wind-shear splitting within evolving atmospheric Kelvin-Helmholtz billows**
D Chapman and K A Browning
April 1997

67. **Cold frontal structure derived from radar wind profilers**
K A Browning, D Jerrett, J Nash, T Oakley and N M Roberts
May 1997

68. **The dry intrusion and its effect on the frontal, cloud and precipitation structure of extratropical cyclones**
K A Browning - Text of invited special lecture at the Spring Conference
of the Meteorological Society of Japan, University of Tsukuba, 22 May 1997

69. **Met. Office Unified Model data, diagnostics, graphics programs, and other observational data available from the JCMM through the aegis of the Universities Weather Research Network (UWERN).** (Plus supplement)
Peter Panagi and Ed Dicks
June 1997

70. **Contributions of the JCMM/Dept of Meteorology Radar Group to the 28th AMS Radar Meteorology Conference.** Austin, Texas
September 1997

71. **Sensitivity of short-range weather forecasts to local potential vorticity modifications**
Meral Demirtas and Alan Thorpe
July 1997

72. **Objective identification of frontal wave cyclones**
T D Hewson
August 1997

73. **Attribution and its application to mesoscale structure associated with tropopause folds**
A J Thorpe
September 1997

74. **The role of the environmental flow in the development of secondary frontal cyclones**
Ian A Renfrew, Alan J Thorpe and Craig H Bishop
September 1997

75. **Potential vorticity: a short history of its definitions and uses**
Alan J Thorpe and Hans Volkert
September 1997

76. **Superposing semi-geostrophic potential vorticity anomalies**
H R Birkett and A J Thorpe
September 1997

77. **Short period forecasting of catchment-scale precipitation.**
Part 1: the role of Numerical Weather Prediction
M A Pedder, M Haile and A J Thorpe
September 1997

78. **Verification of the tracking technique used in an experimental cloud motion wind inferring system**
Z Wang, K A Browning and G A Kelly
October 1997

79. **A preliminary study of Fourier series analysis for cloud tracking with GOES high temporal resolution images**
Z Wang
October 1997

80. **Analysis of an ex-tropical cyclone after reintensifying as a warm-core extratropical cyclone**
K A Browning, G Vaughan and P Panagi
November 1997

81. **A JCMM overview of FASTEX IOPs**
S A Clough, H W Lean, N M Roberts, H Birkett, J-P Chaboureau, R Dixon, M Griffiths, T D Hewson and A Montani
January 1998

82. **Programs for PV inversion and modification**
Meral Demirtas
December 1997

83. **Release of potential shearing instability in warm frontal zones**
D Chapman and K A Browning
February 1998

84. **The European Cloud-Resolving Modelling Programme (EUCREM)**
Summary Report from the coordinator
P W White
April 1998

85. **A frontal wave database**
T D Hewson
April 1998

86. **Layering observed in dropsoundings from IOP 1 of Fronts 92**
S A Clough
May 1998

87. **Use of wind-shear displays for Doppler radar data**
D Chapman and K A Browning
May 1998

88. **Radar estimates of rainfall rates at the ground in bright band and non-bright band events**
T J Smyth and A J Illingworth
June 1998

89. **Correction for attenuation of radar reflectivity using polarisation data**
T J Smyth and A J Illingworth
June 1998

90. **The effects of convection on chemical reactions and precipitation scavenging**
Neil R Gimson
July 1998

91. **How to use the display program DISP**
Nigel Roberts
August 1998

92. **Conceptual models of cyclogenesis**
Adrian T Semple
August 1998

93. **Observations of oblate hail using dual polarisation radar and implications for hail detection schemes**
T J Smyth, T M Blackman and A J Illingworth
September 1998

94. **The semigeostrophic diagnosis of vertical motion. Part I: Formulation and co-ordinate transformations**
Mike A Pedder and Alan J Thorpe
September 1998

95. **The semigeostrophic diagnosis of vertical motion. Part II: Results for an idealised baroclinic wave life cycle**
Alan J Thorpe and Mike A Pedder
September 1998

96. **Convective destabilisation by a tropopause fold diagnosed using potential vorticity inversion**
Morwenna Griffiths, Alan Thorpe and Keith Browning
October 1998

97. **Forecast skill of the ECMWF model using targeted observations during FASTEX**
A Montani, A J Thorpe, R Buizza and P Unden
October 1998

98. **Observations and model simulations of the FASTEX IOP 16 frontal wave - effects of sublimation**
Sid A Clough, Humphrey W Lean, Nigel M Roberts and Richard M Forbes
December 1998

99. **The application of conceptual models in NWP**
Adrian T Semple
January 1999

100. **Mesoscale analysis of arc rainbands in a dry slot**
K A Browning and N M Roberts
January 1999

101. **Interaction of mesoscale tropopause depressions with a warm-core cyclone: observational and model analyses, and sensitivity to analysis errors**
K A Browning, A J Thorpe, A Montani, D Parsons, M Griffiths, P Panagi and E M Dicks
February 1999

102. **The use of water vapour imagery and PV inversion to adjust initial conditions in NWP**
Sean J Swarbrick
February 1999
This report is no longer available; see Internal Report No.108

103. **Summary notes for a lecture course on Waves in the Atmosphere and Ocean**
A A White
March 1999

104. **Results of a questionnaire on the operational value of conceptual models (CMs) of fronts and cyclones**
N M Roberts & M V Young
July 1999

105. **Contributions to the Poster Session at the 1998 UWERN Annual Science Meeting**
assembled by A A White
August 1999

106. **The objective analysis of dropsonde data from FASTEX**
Richard Forbes, Sid Clough, Mark Dixon, Andy Macallan & Nigel Roberts
January 2000

107. *NWP Technical Report No.302*
Implications for Mesoscale Modelling from a Study of the FASTEX IOP 16 Mid-latitude Cyclone
Richard M Forbes, Humphrey W Lean, Nigel M Roberts and Peter A Clark
March 2000

108. *NWP Technical Report No.291*
The use of water vapour imagery and PV inversion to adjust initial conditions in NWP
Final Project Report
Sean J Swarbrick
September 1999

109. *NWP Technical Report No.294*
A guide to aspects of water vapour imagery interpretation: the significance of dry regions
Nigel M Roberts
January 2000

110. *NWP Technical Report No.300*
The relationship between water vapour imagery and thunderstorms
Nigel M Roberts
February 2000

111. *NWP Technical Report No.293*
Holomorphic structures in hydrodynamical models of nearly geostrophic flow
V N Roubtsov and I Roulstone
January 2000

112. *NWP Technical Report No.301*
Multi-sensor synthesis of the mesoscale structure of a cold-air comma cloud system
K A Browning, P Panagi and E M Dicks
March 2000

113. *NWP Technical Report No.307*
Observations of stratospheric air entering the circulation of a polar low
K A Browning and E M Dicks
May 2000

114. *NWP Technical Report No.309*
Wind profiler – Unified Model comparison statistics
Peter Panagi & Ed Dicks
March 2000

115. *NWP Technical Report No.310*
Towards a similarity theory of moist convective updrafts
Olaf Stiller and George C Craig
May 2000

116. *NWP Technical Report No.312*
The mystery of striated cloud heads in satellite imagery
R S Dixon, K A Browning and G J Shutts
April 2000

117. *NWP Technical Report No.313*
MDIAG: a Fortran 90 program to compute diagnostics on pressure levels from Unified Model data on model levels
Peter Panagi
June 2000

118. *NWP Scientific Paper No.56*
Rearrangements of functions with applications to meteorology and ideal fluid flow
R J Douglas
June 2000

119. *NWP Technical Report No.320*
Tests of New Dynamics Model on the FASTEX IOP16 case
Humphrey Lean
September 2000

120. *NWP Scientific Paper 57*
A classification of FASTEX cyclones using a height-attributable QG vertical motion diagnostic
A C L Deveson, K A Browning, T D Hewson
September 2000

121. *NWP Scientific Paper 59*
Measurements of dissipation rate in frontal zones
D.Chapman, K A Browning
August 2000

122. *NWP Technical Report 331*
Not Issued

123. *NWP Technical Report 337*
A Case Study of High Resolution Fog Forecasts with the New Dynamics
P. Clark
November 2000

124. *NWP Technical Report 338*
Comparison of ECMWF Winter-Season Cloud Fraction with Radar Derived Values
Robin J. Hogan, Christian Jakob, Anthony J. Illingworth
January 2001

125. *NWP Technical Report 339*
Deriving Cloud overlap statistics from radar
Robin J. Hogan, Anthony J. Illingworth
January 2001

126. *NWP Technical Report 344*
Results from simulations of an organised convective event using the New Dynamics at 12, 4 and 2km resolution.
Nigel Roberts
January 2001

127 *NWP Technical Report 348*
A North Atlantic Survey of Cyclogenesis in 1999: Unified Model Performance in Short Range Forecasts & The Relationship Between Potential Vorticity, Water Vapour Imagery and Analysis Accuracy.
Adrian Semple
March 2001

128 NWP Scientific Paper 61
Are there higher-accuracy analogues of semigeostrophic theory?
Ian Roulstone, Michael E. McIntyre
June 2001

129 NWP Scientific Paper 62
Stacked slantwise convective circulations
K A Browning, D Chapman, R S Dixon
April 2001

130 NWP Technical Report 357
A Meteorological Assessment of the Geostrophic Co-ordinate Transform and Error Breeding System when used in 3D Variational Data Assimilation.
Adrian Semple
June 2001

131 NWP Scientific Paper 63
The dynamics of a mid-latitude cyclone with very strong latent heat release
Farhang Ahmadi-Givi, George Craig
July 2001

132 NWP Scientific Paper 64
A Study of the Effects of Horizontal and Vertical Resolution in the New Dynamics representation of FASTEX IOP16
Humphrey Lean
October 2001

Met Office Joint Centre for Mesoscale Meteorology Department of Meteorology
University of Reading PO Box 243 Reading RG6 6BB United Kingdom
Tel: +44 (0)118 931 8425 Fax: +44 (0)118 931 8791
www.metoffice.com